Earth-Science Reviews 214 (2021) 103545

Contents lists available at ScienceDirect

Earth-Science Reviews

journal homepage: www.elsevier.com/locate/earscirev

Review Article

Movable oil content evaluation of lacustrine organic-rich shales: Methods and a novel quantitative evaluation model

Tao Hu [a,b,*], Xiongqi Pang [a,b,*], Fujie Jiang [a,b,*], Qifeng Wang [c,**], Xiaohan Liu [a,b], Ze Wang [a,b], Shu Jiang [d], Guanyun Wu [a,b], Caijun Li [a,b], Tianwu Xu [e], Maowen Li [f], Jiwang Yu [a,b], Chenxi Zhang [a,b]

[a] State Key Laboratory of Petroleum Resources and Prospecting, Beijing 102249, China
[b] College of Geosciences, China University of Petroleum (Beijing), Beijing 102249, China
[c] Research Institute of Petroleum Exploration and Development, PetroChina, Beijing 100083, China
[d] Energy & Geoscience Institute, University of Utah, Salt Lake City, UT 84108, USA
[e] Research Institute of Exploration and Development, Zhongyuan Oilfield Company, SINOPEC, Puyang 457001, China
[f] State Key Laboratory of Shale Oil and Shale Gas Resources and Effective Development, Sinopec Petroleum Exploration and Production Research Institute, Beijing 100083, China

ARTICLE INFO

Keywords:
Movable oil content
Lacustrine organic-rich shale
Controlling factors
Quantitative estimation model
Shahejie Formation
Dongpu Depression
Bohai Bay Basin

ABSTRACT

Lacustrine shale oil resources are abundant and play important roles in maintaining a sustainable economy. The uncertainty in the movable oil content of organic-rich shales with strong heterogeneity is the greatest risk in their exploration. Various methods exist for movable oil content evaluation, but they present many challenges, especially insufficient accuracy, complicated test procedures, high costs, and limited application. In this study, an extensive review of the theories, techniques, and methods of movable oil content evaluation and their merits and demerits for lacustrine shales were conducted. Then, taking the lacustrine shale of the Paleogene Shahejie Formation (50.5–33 Ma) of the Dongpu Depression, Bohai Bay Basin, as an example, the multi-step Rock-Eval pyrolysis method combined with light hydrocarbon calibration was utilized to evaluate the movable oil content Subsequently, key factors controlling movable oil content were investigated, including organic matter richness, type, and thermal maturity, quartz content, clay mineral content, pore volume, and specific surface area. Both the systematic cluster analysis results and regression standardization coefficients indicate that the total organic carbon content, pore volume, and specific surface area are the main controls on movable oil content. Finally, a quantitative estimation model for movable oil content was established and validated using a statistical product and service solutions modeling. This study improves the understanding of shale oil enrichment laws and provides a novel and practical quantitative model for movable oil content estimation in lacustrine organic-rich shales across the world.

1. Introduction

Oil and gas are the most important primary energy sources in the world, and it is expected that in 2040, oil and gas will continue to account for more than 50% of the global primary energy supply (Exxon, 2018; EIA 2019a). In the context of the conventional oil and gas resource shortage, this energy balance will potentially be maintained mainly by shale oil and gas contributions (Hughes, 2013; Hopkins 2017). Inspired by the development of shale gas and the impact of lower natural gas prices, investors are increasingly focusing on shale oil (Kirschbaum and Mercier 2013). In the last decade, the "shale oil revolution" in the US has had profound implications for the US economy (Mănescu and Nuño 2015; Exxon, 2018). Although the US is most likely to be the dominant shale oil producer for the next decade, recoverable shale oil resources outside the US are estimated to be five times that of the US (EIA, 2013; Mănescu and Nuño 2015). Accelerating shale oil utilization may be a key factor of guaranteeing a sustainable global oil energy supply (Hughes, 2013; Hopkins 2017; Jin et al. 2019; Zhao et al., 2020a).

* Corresponding authors at: State Key Laboratory of Petroleum Resources and Prospecting, Beijing 102249, China.
** Corresponding author.
E-mail addresses: thu@cup.edu.cn (T. Hu), pangxq@cup.edu.cn (X. Pang), jiangfj@cup.edu.cn (F. Jiang), wangqifeng1021@163.com (Q. Wang).

https://doi.org/10.1016/j.earscirev.2021.103545
Received 24 September 2020; Received in revised form 28 January 2021; Accepted 30 January 2021
Available online 4 February 2021

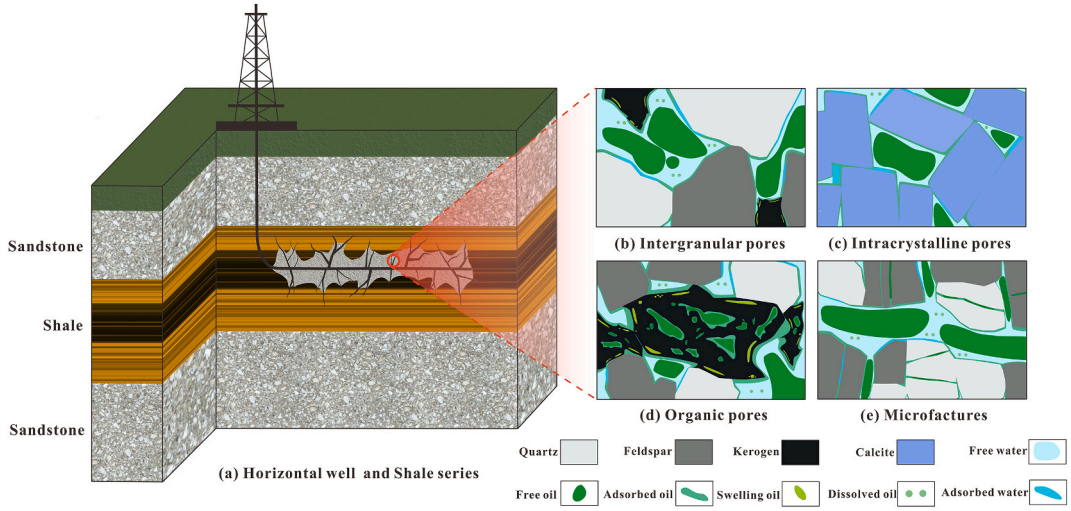

Fig. 1. Occurrence state model of adsorbed oil, free oil, swelling oil, and dissolved oil in shales.

The total amount of shale oil on Earth is considerable (EIA, 2013, 2019a; Mănescu and Nuño 2015; Jin et al. 2019; Zhao et al., 2020a, b). However, shale oil utilization has been successful only in North America. The US produced 2.349 billion barrels of shale oil in 2018, accounting for 64.7% of the total US oil production (EIA 2019b). US shale oil production is expected to reach 9.46 million barrels per day (b/d) in 2040, accounting for 67.3% of the total US oil production (EIA 2019a). Although other countries have abundant shale oil resources (Mănescu and Nuño 2015), they are in the preliminary stage of shale oil exploration and development, and current production is limited (Jin et al. 2019; Zhao et al., 2020a, b). The successful exploration and development of shale oil in the US is attributed to the shale oil being in mainly tight sandstone or carbonate reservoirs that are interbedded with shale in marine sediments; additionally, this shale oil has a relatively high thermal maturity, high contents of light hydrocarbons, and a high movable oil content (Jarvie, 2012, 2014; Kuhn et al. 2012; Larter et al. 2012). In contrast, shale oil in other countries, especially in China, mainly occurs in relatively pure shale in lacustrine deposits (Song et al. 2013; Zhang et al. 2014). Due to greater sensitivity to high frequency climatic variability and biota origins within lacustrine systems (Katz 1995; Katz and Lin 2014), lacustrine shales display strongly heterogenous biota, mineral composition, and textures. Furthermore lacustrine oils are waxier contain less but variable light hydrocarbons (Katz 1990; Katz and Lin 2014). Therefore, compared with marine oil, lacustrine oil is more viscous and hence less movable (Nie et al. 2016; Wang et al. 2019a). For example, in well Boyeping 1 in the Shengli Oilfield, after two fracturing procedures, the initial daily oil yield was only 8.22 m^3 and quickly reduced to 1.6 m^3, the cumulative production was only approximately 100 m^3 (Lu et al. 2016). The Biye HF1 well in the Biyang Depression of the Henan Oilfield was the breakthrough well for lacustrine shale oil exploration in China and obtained a daily oil yield of 23.6 m^3 after staged fracturing, but the daily oil yield soon decreased to 1 m^3. In addition, the daily oil yields of well Biye HF2 decreased from an initial yield of 32 m^3 to 1 m^3 (Ma et al., 2012; Zhang et al. 2012). The limited production might be related to the selection of poor drilling locations, which are mainly due to a lack of understanding of shale oil enrichment rules, especially movable oil content (Lu et al. 2016).

Generally, oil occurs in four states in shale: adsorbed, free, swelling, and solution (O'Brien et al., 2002; Jarvie, 2012; Larter et al. 2012; Jiang et al. 2016; Li et al. 2016a). The adsorbed oil exists in a high density "solid-like" form through the interaction of van der Waals and Coulomb forces at the surface of organic matter and minerals and has no fluidity (Curtis, 2002a, b). Free oil occurs in large pores and fractures. Due to a certain distance between the oil and minerals, it is not bound by intermolecular interaction forces and occurs in pores and fractures in the form of spherical oil droplets. Therefore, free oil can flow (O'Brien et al., 2002). Swelling oil refers to the oil "embedded" in the organic matter structures. The oil molecules are surrounded by kerogen molecules, and cannot flow (Van 2000; Li et al. 2016a). Dissolved oil is mainly dissolved in water and natural gas. However, due to the low water and gas contents in shale and the extremely low oil solubility, the dissolved oil content is limited and can be ignored (Zhang et al. 2014). Fig. 1 illustrates the four kinds of shale oil. Under current technical conditions, only shale oil with a free state is a movable and exploitable resource (Jarvie, 2012; Larter et al. 2012). For shale oil exploration, the movable oil content in shale directly determines the enrichment degree of the shale oil resources, and the higher the enrichment degree, the higher the producibility will be (Jarvie, 2012; Larter et al. 2012). For the high wax and viscous oil of the heterogenous lacustrine shales (Katz 1990; Katz and Lin 2014), how much oil is movable? What are the factors that truly influence the movable oil content? The answers to these two questions influence how much of the lacustrine shale oil resources can be extracted, given the available technology (Lu et al. 2016). Accurate evaluation of the movable oil content is one of the key scientific problems that is required to be solve to achieve efficient exploration and development of lacustrine shale oil. Some methods for movable oil evaluation in lacustrine shale have been proposed by researchers, but still have some limitations (Section 2).

Recently, large lacustrine shale oil resources were discovered in the Paleogene organic-rich shales in the Dongpu Depression (DD), Bohai Bay Basin, eastern China. These shales have the basic elements required for conducting a movable oil evaluation. Since the oil discovery in Paleogene shales in 1976, shale oil exploration has continued and many shale cores samples have been collected. Also, a shale oil exploration well PS 18–1 exhibited excellent daily production of 430 m^3 in the Liutun Sag (Zhang et al. 2015). However, in the same sag and formation, only weak oil shows were observed in the PS 18–8 well, drilled only 800 m from the PS 18–1 well. These results provide excellent targets for a comparative study of the shale oil content. These shales are highly heterogeneous and vary in lithofacies (Shao et al. 2018; Li et al. 2020b). The organic matter richness, mineral and oil contents of this shale are significantly different among the different lithofacies, so it is suitable for analyzing key factors controlling oil content variability (Wang et al. 2015a, 2020a; Shao et al. 2018; Li et al. 2020a).

A brief review of the theories, techniques, and methods for movable oil content evaluation and their limitations for organic-rich shales is presented in this study. Following this review, the Paleogene shales in the DD are used as an example of the multi-step Rock-Eval pyrolysis

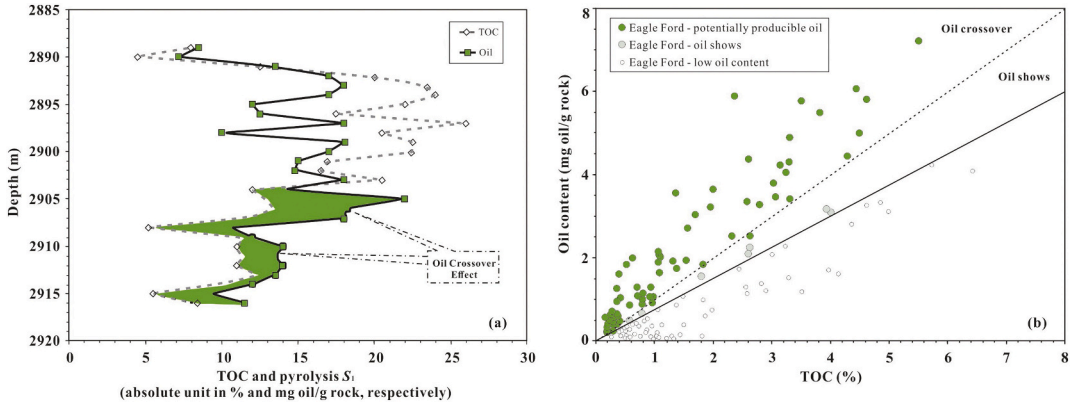

Fig. 2. Examples of oil crossover effect in productive marine shale oil plays (Lopatin et al. 2003; Jarvie, 2012).

method (MREPM) combined with light hydrocarbon calibration to evaluate movable oil content. Key factors controlling of movable oil content are identified. Using statistical product and service solutions (SPSS) numerical modeling, a quantitative estimation model for movable oil content was established and validated. This study improves the understanding of oil enrichment rules in lacustrine shale oil plays and provides a novel and practical model for movable oil content evaluation based on existing big test data from lacustrine organic-rich shales across the world. This model and its establishing procedures can also be a reference for marine shale oil evaluation.

2. Review of movable oil content evaluation methods

2.1. Oil saturation index (OSI) method

The OSI (OSI = S_1/TOC × 100, where TOC is the total organic carbon content) index was first used for conventional oil and gas exploration in North America. For a conventional reservoir, OSI values greater than 100 mg HC/g TOC indicate oil shows (Jarvie and Baker 1984; Behar et al. 2002; Lopatin et al. 2003). Jarvie (2012) calculated the OSI values of the producing layers in US shale oil plays and found that layers with OSI values greater than 100 HC/g TOC have commercial potential (Fig. 2) (Jarvie, 2012, 2014). Subsequently, he proposed that the oil cannot migrate effectively with OSI values less than 100 HC/g TOC and that oil is movable with OSI values higher than 100 HC/g TOC; this was referred to as oil crossover effect (Jarvie, 2012). This method considers two factors when the OSI values exceed 100 HC/g TOC: ① The oil generated by the shale has met its residual adsorption capacity (Pepper 1992; Jarvie et al. 1995). ② The shale has open fracture networks that facilitates oil flow (Jarvie, 2012, 2014). Therefore, OSI = 100 mg HC/g TOC can be taken as the lower limit of shale oil mobility, and the excess part to 100 mg HC/g TOC is the movable oil content. At present, the OSI method has achieved excellent results in marine systems (Jarvie, 2012, 2014) and has also been applied to lacustrine systems, such as the Songliao (Cao et al., 2017), Junggar (Hu et al. 2018a), and Bohai Bay Basins (Wang et al. 2015a, 2015c).

However, the OSI method has four limitations: ① Compared with marine shales, lacustrine shales are highly heterogeneous (Katz and Lin 2014; Zou et al. 2019). When the pyrolysis S_1 and TOC are both low, the OSI can exceed 100 mg HC/g TOC. ② The 100 mg HC/g TOC was proposed based on statistical analyses of marine shale oil yield data, but there are many factors affecting shale oil mobility, such as organic matter richness, type, and thermal maturity, mineral composition, shale textures, and pore space characteristics, which are significantly different among shales of different lithofacies. Therefore, it is improper to use a constant to evaluate the threshold of movable oil content of heterogeneous lacustrine shales. Some studies showed that the residual oil contents in lacustrine shales vary greatly, ranging from 30 to 180 mg HC/g rock (Philippi 1965; Hunt 1967; McAuliffe 1978; Xue et al. 2015), even reaching 200 mg HC/g rock (Pepper and Corvi, 1995, b).

2.2. Grading evaluation method (GEM)

Shale is more difficult to exploit than conventional reservoirs because of low porosity and low permeability. Previous studies mainly utilized the GEM to evaluate lacustrine shale oil resources. Zhang et al. (2012) proposed classification standards for grading lacustrine shale oil resource in terms of thickness, TOC, thermal maturity, burial depth, oil content, frackability, and formation pressure. Specifically, oil content of 0.10%–0.15%, 0.15%–0.20%, and greater than 0.20% indicate prospective, favorable, and excellent shale oil resource (Zhang et al. 2012). Whereas these standards lack the support of practical data (Lu et al. 2012).

Lu et al. (2012) analyzed the geochemical parameters of shale oil

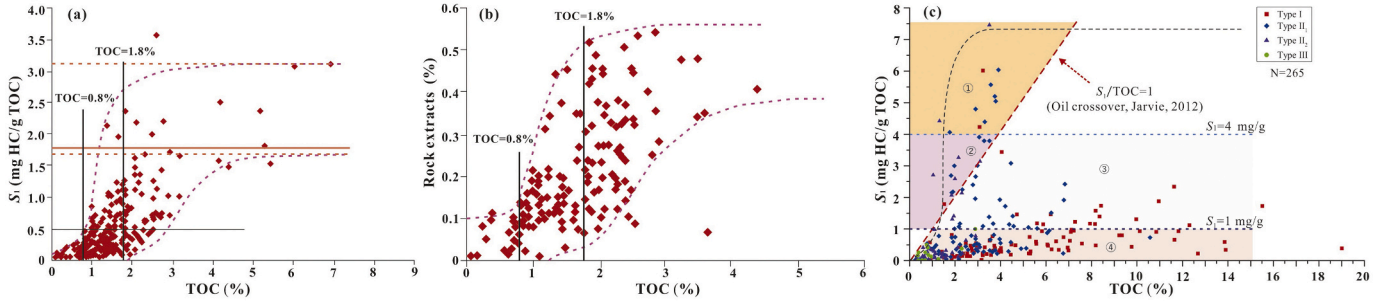

Fig. 3. The grading evaluation standards for shale oil resources by using the "trichotomy" of the correlation between oil content (pyrolysis S_1 or rock extracts) and TOC contents. (a) and (b) Qingshankou Formation shales in the southern Songliao Basin (Lu et al. 2012); (c) Lucaogou Formation shales in Jimusar Sag in Junggar Basin (Hu et al. 2018a).

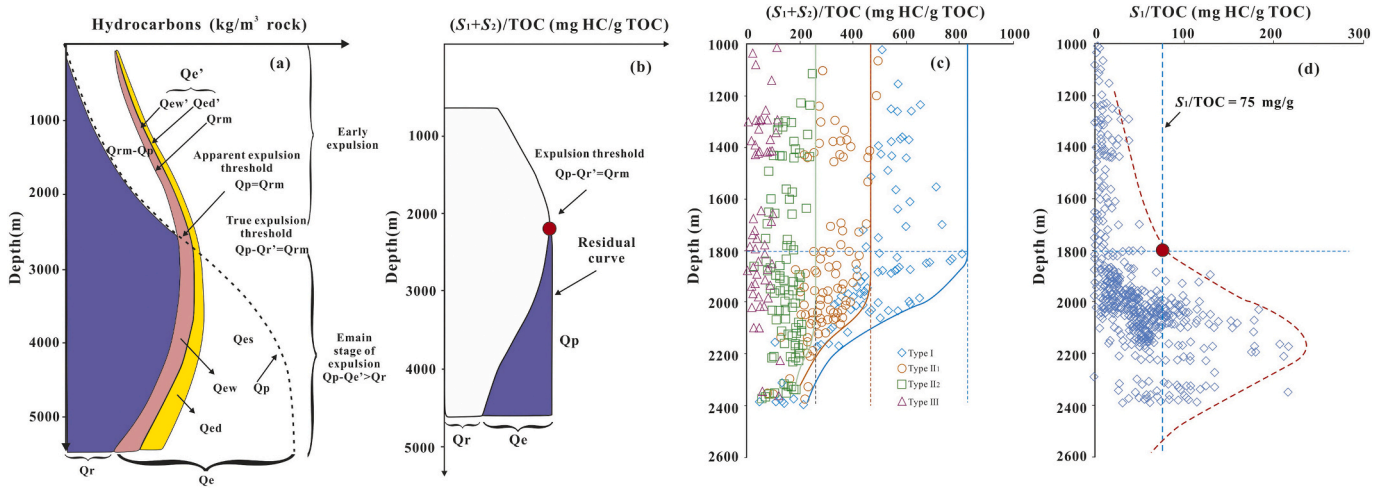

Fig. 4. Movable oil contents evaluated by hydrocarbon expulsion threshold method. (a) and (b) Conceptual model for HET identification (Pang et al., 1993a, b, 2005; Peng et al. 2016). Q_p = hydrocarbon generation amount; Q_e = amount of hydrocarbon expelled; Q_r = amount of residual hydrocarbon; Q_{rm} = minimal amount of hydrocarbon needed to saturate the source rock porosity; Q_{ew} = amount of hydrocarbon dissolved in water; Q_{ed} = amount of hydrocarbon diffused out of source rock; Q_{es} = amount of hydrocarbon expelled in separate phase; $Q_{e'}$ = amount of hydrocarbon expelled in early expulsion; $Q_{ew'}$ = amount of hydrocarbon dissolved in water in early expulsion; and $Q_{ed'}$ = amount of hydrocarbon diffused out of source rock in early expulsion. (c) and (d) Movable oil contents evaluation in Qingshankou Formation shales in southern Songliao Basin (Xue et al. 2015).

plays in the Songliao (Qingshankou Formation (Fm.), vitrinite reflectance (*Ro*) of 0.7%–1.3%), Hailaer (Nantun Fm., *Ro* of 0.7%–1.0%), Yitong (Shuangyang Fm., *Ro* of 0.6%–1.3%), and Bohai Bay Basins (Shahejie Fm., *Ro* of 0.5%–1.1%) and divided the shale oil into dispersed, inefficient, and enriched resources, by using the "trichotomy" of the correlation between oil content (pyrolysis S_1 or rock extracts) and TOC content. The pyrolysis S_1 and rock extracts show three classes with increasing TOC (Fig. 3a and b). ① The TOC content is low, and the pyrolysis S_1 is low and stable with increasing TOC content. For the shales with low TOC content, the oil generated is small. ② The TOC content is high, and the pyrolysis S_1 is high and stable with increasing TOC content. For the shales with high TOC content, the oil generated amount is great and can saturate the shale. Further generated oil will be expelled and hence the pyrolysis S_1 is basically the same. ③ The TOC content is medium, and the pyrolysis S_1 increases rapidly with increasing TOC content. For the shales with medium TOC, the oil generated is not small but still insufficient to reach residual adsorption capacity. With increasing TOC, further generated oil will retain in shale pores and fractures and thus pyrolysis S_1 increases gradually (Lu et al. 2012). The three classes correspond to dispersed, inefficient, and enriched resources, respectively. Only enriched resources provide movable shale oil resources that can be currently exploited. Inefficient resources are those that might be exploited after future technological breakthroughs are made, while dispersed resources may never be exploited efficiently. Compared with movable oil content evaluation considering only pyrolysis S_1 or rock extracts, the GEM considers the oil adsorption. GEM utilizes the absolute values of the pyrolysis S_1, rock extracts, and TOC contents in the oil content evaluation, hence avoiding the limitations of the OSI method, such as the misjudgment situation when both pyrolysis S_1 value and TOC content are low but with great OSI value. However, this method still uses TOC and pyrolysis S_1 to grade shale oil resources, and whether enriched shale oil resources are movable is still uncertain. Therefore, GEM only identifies optimal target, and whether it will produce economic yields of shale oil remains unclear.

In view of the above problems, some researchers have proposed an improved GEM, aiming to establish the grading evaluation standard for shales with different organic matter types (Fig. 3c) (Li et al. 2015a; Hu et al. 2018a). First, classify the shale types in terms of kerogen types. Second, combine the OSI method and GEM to analyze the difference between the absolute and relative oil contents of shale with different types and finally establish the improved GEM. The improved GEM not only reduces uncertainty in the movable oil content evaluation of heterogeneous lacustrine shale, but also improves the accuracy of the evaluation by utilizing GEM. However, this method still has some problems, such as whether it is appropriate to use the marine shale movable oil threshold value OSI = 100 mg/g for determining the mobility of lacustrine shale oil.

2.3. Hydrocarbon expulsion threshold method (HETM)

Based on mass balance principle, utilizing the organic matter within shales that could be converted into hydrocarbons, the mass must be certain if there is no material exchange with the outside during thermal evolution. Hydrocarbon generation potential is determined by three components: unconverted organic matter or kerogen, residual, and expelled hydrocarbons (Momper 1978; Pang et al., 1993a, b, 2005). Therefore, regardless of how organic matter generates hydrocarbons, with increasing thermal maturity, generated hydrocarbons will begin to migrate out in a free state when the generated hydrocarbon exceeds that needed to meet retention capacities, including self-absorption, swelling, pore water dissolution, oil dissolution, gas dissolution, residual pore and fracture capacity, and capillary plugging. The thermal maturity or burial depth at which hydrocarbons begin to migrate outward in a free state refers to hydrocarbon expulsion threshold (HET), which can be determined by hydrocarbon generation potential method (Fig. 4a and b) (Pang et al., 1993a, b, 2005; Hu et al., 2016).

Xue et al. (2015) and Wang et al. (2015d) hold that the OSI value of shale at the HET refers to the oil mobility threshold (Fig. 4c and d), and the difference between the OSI and the threshold values refers to movable oil content (Xue et al. 2015). Due to differences among HETs of the shale deposited in different sedimentary environments (Pang et al., 1993a, b, 2005), different types of shale have different oil mobility thresholds. However, when shales start to expel hydrocarbons after the HET is exceeded, the residual hydrocarbons need to exceed not only the oil swelling and adsorption capacities but also the pore water dissolution, oil dissolution, gas dissolution, and free hydrocarbon retention in pores and fractures (Pang et al., 1993a, b, 2005). Therefore, the HETM ignores the free oil in pores and fractures, which is the main components

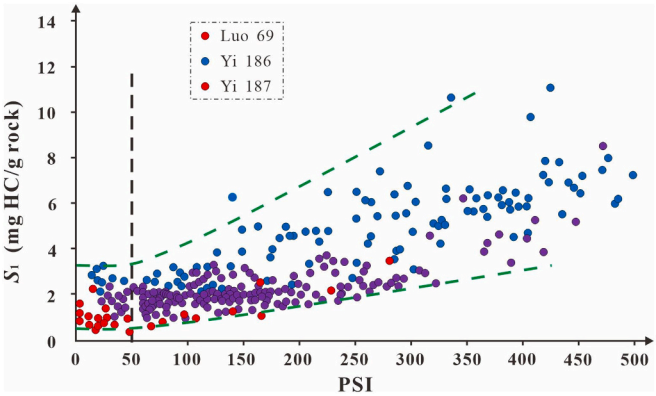

Fig. 5. Movable oil content evaluation of pore oil saturation method by analyzing pore saturation index and pyrolysis S_1 (Su et al., 2017a, b).

of movable oil. Hence, this method underestimates the actual movable oil content.

2.4. Pore oil saturation method (POSM)

In principle, the POSM is the closest method to the conventional resource calculation method (Eq. 1), and it has been applied in the Bonan Depression, Bohai Bay Basin (Song et al. 2013).

$$N = 100 \times A \times h \times \varnothing \times S_O \times \rho_0 / B_{oi} \quad (1)$$

N is the total geological oil reserves; A is the oil-bearing area; H is the effective thickness; Φ is the effective porosity; So is the oil saturation; ρ_0 is the oil density; Boi is the oil volume coefficient.

Su et al. (2017a, b) analyzed the correlation among the OSI, porosity, and permeability of shales, and found the OSI values are positively correlated with porosity but negatively correlated with $(K/(\Phi \times 100))^{1/2}$ and concluded that the movable oil content is negatively correlated with permeability. The higher the permeability, the easier it is for oil to migrate and expel, thus leading to a decrease in oil content. Based on the above analyses, pore saturation index (PSI) was proposed to evaluate movable oil content (Eq. 2) in Zhanhua Sag, Bohai Bay Basin (Su et al., 2017a, b). Results show that pyrolysis S_1 basically remains unchanged when the PSI is less than 50, while increases gradually when the PSI is greater than 50, hence PSI = 50 was defined as the critical lower limit for shale oil mobility (Fig. 5). With this value, shale oil layers can be evaluated as having low (<50) and high (>50) oil contents. The higher the PSI value is, the higher the oil content is (Su et al., 2017a, b).

$$PSI = \frac{S_1}{TOC \times 100} \sqrt{\frac{\varnothing \times 100}{K}} \quad (2)$$

S_1 is the hydrocarbons retained in the shale; TOC is the total organic carbon content; Φ is the porosity; K is the permeability.

However, the POSM has four limitations: Test accuracy of shale porosity and oil saturation is affected by many factors. For example, a high-temperature distillation process (i.e., Dean Stark extraction) is necessary before porosity and oil saturation testing, but some labile fraction of organic matter will be dissolved in this process, resulting in an overestimation of porosity and oil saturation (Modiea and Lapierre 2012). ② Strict core requirements are needed for porosity and oil saturation tests, such as size, fracture development degree, and preservation condition. ③ The PSI is an empirical threshold for oil content obtained by statistical analysis and cannot evaluate movable oil content quantitatively. ④ Identification of the PSI threshold assumes permeability is negatively correlated with oil content, but in fact, shales are low-porosity and low-permeability reservoirs, and the movable oil mainly exists in large pores and fractures. Therefore, the PSI mainly reflects the oil retained in matrix pores.

2.5. Multistep rock-eval pyrolysis method (MREPM)

Shale oils with different occurrence states have different molecular thermal volatilization characteristics (Maende et al. 2017). Lower molecular weight oil compounds are more likely to be thermally released than higher molecular weight compounds, shale oil in large fractures and pores is more easily pyrolyzed than that in small pores, and free oil is more likely to be thermally released than adsorbed or mixed oil (Jiang et al. 2016). Therefore, pyrolysis can be used to quantitatively evaluate the oil with different occurrence states. Traditional Rock-Eval pyrolysis heats the shale from room temperature to 550 °C or 600 °C at a rate of 20 °C/min. It is considered that the S_1 peak appearing before 300 °C represents free oil that has not yet been discharged, and the S_2 peak appearing after 300 °C represents oil generated by further kerogen pyrolysis. The S_1 is easy to extract by weak-polar dichloromethane, so it is regarded as free oil (movable oil) (Sanei et al. 2015; Jiang et al. 2016). However, further studies found that the oil generated by shale cannot all be evaporated before 300 °C and that S_2 also contains some free oil, adsorbed oil, and swelling oil. Therefore, traditional Rock-Eval pyrolysis cannot accurately quantify free oil (Jiang et al. 2016). In 1989, by adjusting the heating procedures of the Rock-Eval instrument, oil content of sandstone was quantitatively analyzed (Wu et al. 2000). At pyrolysis temperatures of 90 °C, 200 °C, 200–250 °C, 350–450 °C, 450–600 °C, and 600 °C, the obtained components were S_0 (natural gas), S_{11} (gasoline), S_{21} (kerosene and diesel), S_{22} (wax and heavy oil), S_{23} (colloidal and asphaltic), and S_4 (residual carbon). The sum of S_{11}, S_{21}, S_{22} and S_{23} was total oil content. Sanei et al. (2015) developed an adapted method, called the extended slow heating (ESH) cycle, to characterize the organic constituents of unconventional tight siltstone reservoirs, in which the heating rate was slowed to 10 °C per minute over an extended temperature range (from 150 to 650 °C). This splits the traditional S_1 and S_2 peaks into three peaks: (S_{1ESH}) free light oil, (S_{2aESH}) fluid-like hydrocarbon residue, and (S_{2bESH} + residual carbon) solid bitumen. Compared with sandstone, shale under experimental temperatures has adsorbed, swelling, and pyrolysis hydrocarbon fractions. Hence, the oil content evaluation method of sandstone cannot be applied to shale.

Like the analysis of the oil content in sandstone, shale oil with different occurrence states can be quantitatively characterized by adjusting heating program. Romero-Sarmiento et al. (2016) proposed the shale play method for estimating shale oil contents, splitting the S_1 peak measured by traditional Rock-Eval pyrolysis into two peaks: S_{h0} and S_{h1}. The S_{h0} and S_{h1} are assigned to lighter and heavier thermovaporized hydrocarbons released between 100 and 200 °C and 200–350 °C, corresponding to free (aliphatic) and adsorbed (aromatic) hydrocarbons. Analogously, Maende et al. (2017) utilized the HAWK pyrolysis instrument's Petroleum Assessment Method (HAWK-PAM) and advanced pyrolysis plots that model sorbed versus total oil yields. By using HAWK-PAM, the S_1 peak is split into 4 peaks, including S_{Oil-1} (at 50 °C), S_{Oil-2} (at 100 °C), S_{Oil-3} (at 100–180 °C), and S_{Oil-4} (at 180–350 °C). The first three correspond to saturate and aromatic hydrocarbons and the last one refers to heavy and polar components. However, the above two methods have two limitations: The oil fractions correspond to which peaks are movable oil are uncertain. Further works are still needed to evaluate with precision of the type of hydrocarbons detected by each new acquired Rock-Eval peaks. ② By being subjected to volatile hydrocarbons losses, this too is incapable of evaluating the actual movable oil contents of shales (Espitalié et al. 1977; Lafargue et al., 1998; Behar et al. 2001; Michael et al. 2013).

Jiang et al. (2016) improved the traditional Rock-Eval pyrolysis and established the MREPM for shale oil evaluation in different states by comparing pyrolysis chromatography results obtained before and after dichloromethane extraction. Specifically, S_{1-1} was tested at a constant temperature of 200 °C for 1 min. Then, the temperature was raised to 350 °C at 25 °C/min, and the constant temperature was held for 1 min to test S_{1-2}. The temperature was raised to 450 °C at 25 °C/min to test S_{2-1}.

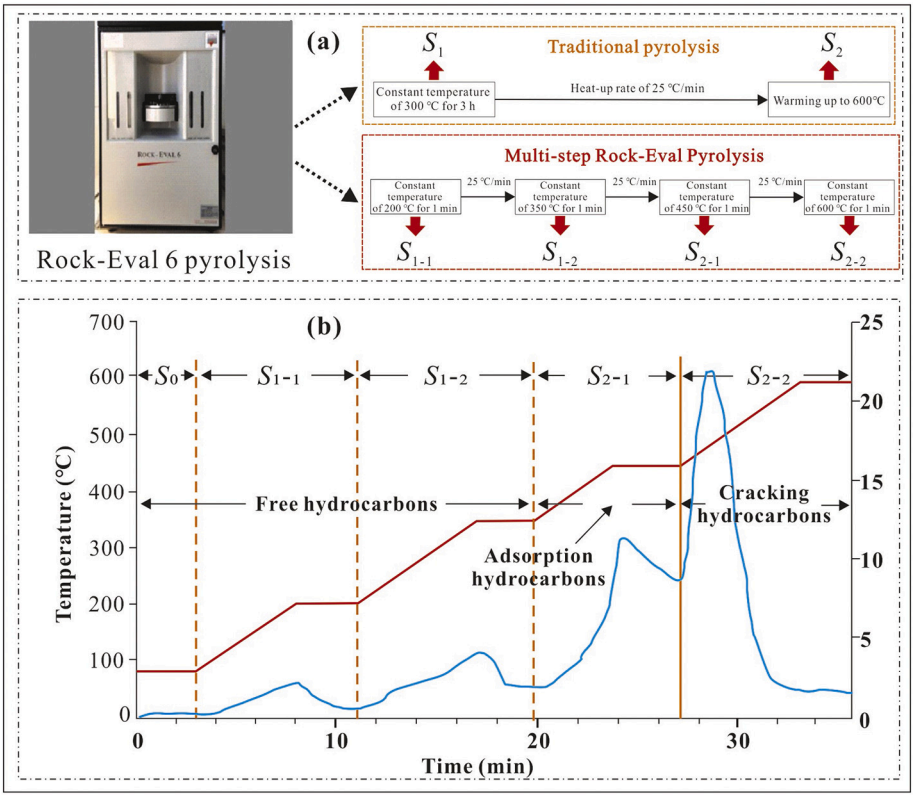

Fig. 6. Test procedures and parameter meaning of Multistep Rock-Eval pyrolysis method (Jiang et al., 2016).

Finally, the temperature was increased to 600 °C at 25 °C/min to test S_{2-2}. S_{1-1} is light oil and represents practical movable oil content, S_{1-2} is mainly light and medium oil and represents the adsorbed oil content (heavy oil and swelling oil), S_{2-1} is mainly heavy oil and gelatinous asphaltene, and S_{2-2} is hydrocarbon generated by kerogen. The sum of S_{1-1} and S_{1-2} is the maximum movable oil content, and the sum of S_{1-1}, S_{1-2} and S_{2-1} is the total oil content in the shale (Fig. 6) (Jiang et al. 2016).

This method can be used to quantitatively evaluate the movable oil content. However, it should be noted that all methods used to obtain the free oil content through laboratory analysis would result in significant light hydrocarbon loss during core preservation and sample preparation (Espitalié et al. 1977; Lafargue et al., 1998; Behar et al. 2001; Michael et al. 2013). Therefore, when using the MREPM to evaluate movable oil, light hydrocarbon calibration is necessary.

2.6. Multi-step solvent extraction method (MSEM)

Traditional Soxhlet extraction is generally used to evaluate soluble organic matter content in rocks. However, it is difficult to distinguish the free, adsorbed, and swelling oil fractions in shale.

Based on the different occurrence spaces and molecular polarities of oil, the occurrence space for free oil is relatively large, resulting in strong contact between the free oil and extraction solvent, so the free oil is easy to extract. Oil occurring in micropores and kerogen or adsorbed on the kerogen surface is difficult for the solvent to reach and thus difficult to extract. In addition, free oil generally features weak molecular polarity and is easy to extract, while adsorbed oil generally features strong polarity and is difficult to extract. Therefore, solvents with different polarities can be used to extract shale samples in bulk or crushed to obtain oil with different occurrence states (Qian et al. 2017). Many studies have been conducted on quantitative analyses of the oil content of different occurrences by combining various polar solvents. For example, the combination of chloroform, hydrochloric acid and hydrofluoric acid was used to divide extraction of carbonate powder samples into free, carbonate composite, and mineral adsorption states (Guan et al. 1998; Wang and Cheng 2000). Because the mineral composition, petrophysical properties, and organic matter enrichment mechanism of shale are different from those of carbonate rocks (Cai et al. 2007; Zhu and Cai 2012). It is necessary to reveal the actual occurrence state of soluble organic matter in the shale step by step with different polarity solvents to obtain oil contents with different occurrence states (Qian et al. 2017). Qian et al. (2017) improved the solvent separation method by utilizing the combination of different polar solvents and extraction methods (Table 1). The oil extracted in steps 1 and 2 is free oil. In step 3, the extracts are adsorbed oil that was adsorbed on the kerogen and small molecular oil within the internal network structure of the kerogen. The oil extracted in step 4 is mainly soluble organic matter containing many

Table 1
Solvent combination and sample status during different test steps of Multi-step solvent extraction method (Qian et al. 2017).

Extraction sequences	Sample form	Solvent system	Solvent amount/ (ml·g^{-1})	Extraction ways
Step 1	Whole piece (1 cm^3)	Dichloromethane/ Methanol (93:7)	0.4	Ultrasonic cold extraction
Step 2	Blocks with lengths of 0.1 and 0.5 cm	Dichloromethane/ Methanol (93:7)	0.4	Ultrasonic cold extraction
Step 3	150 mesh powder	Dichloromethane/ Methanol (93:7)	0.4	Ultrasonic cold extraction
Step 4	150 mesh powder	Tetrahydrofuran/ Acetone/Methanol (50:25:25)	0.15	Ultrasonic cold extraction

Notice: The amount of solvent is the volume of solvent used per gram of rock.

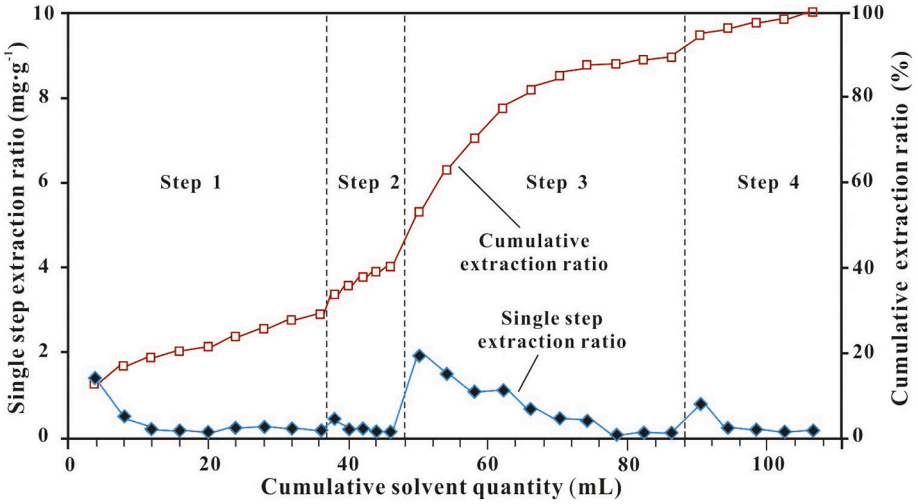

Fig. 7. Test procedures for multi-step solvent extraction method (Qian et al. 2017).

polar components adsorbed on the surface of minerals and is mainly adsorbed oil (Fig. 7) (Qian et al. 2017).

The MSEM has three limitations: Similar to MREPM, significant light hydrocarbon loss occurs during core preservation and sample preparation (Espitalié et al. 1977; Lafargue et al., 1998; Behar et al. 2001; Michael et al. 2013). ② In the process of analysis, it involves the preparation of bulk and powder samples and requires ratio tests of various polar solvents. This is complex, complicated, and expensive and therefore limited to sample studies (Zhu et al., 2019a). ③ The extraction process cannot completely realize the selective separation of oil with different occurrence states. In addition, a certain dynamic transformation of the oil with different occurrence states occurs in the shale. The range of solvents and extraction methods used may cause variations in experimental data (Qian et al. 2017).

2.7. Free hydrocarbon difference method (FHDM)

Aiming at the heterogeneity of lacustrine shale, the FHDM first divides the shale into small hydrocarbon generation and expulsion units, and then calculates original hydrocarbon generation amount of each unit based on the hydrocarbon generation principle of kerogen obtained by thermal simulation experiments. The difference between the original hydrocarbon generation amount and actual oil content refers to free hydrocarbon difference (δS_1), which can be used to evaluate movable oil content (Li et al. 2016b, 2019a). The procedures are as follows: The vitrinite reflectance (*Ro*) of the shale samples is calculated based on the regression formula of *Ro* with depth. ② According to pyrolysis data or kerogen organic elemental data, organic matter types are classified (I, II_1, II_2, III). ③ Thermal simulation experiments are performed to obtain hydrocarbon generation rate (HCGR) of shale with different organic matter types. The HCGR is multiplied by TOC to obtain hydrocarbon generation quantity (HCGQ). ④ The HCGQ minus the corrected pyrolysis S_1 refers to δS_1 (Li et al. 2016b, 2019a).

$\delta S_1 < 0$ (Type A) indicates that the original HCGQ is less than the actual free hydrocarbon amount, corresponding to an influx of hydrocarbon. For Type A shale, the TOC content and original HCGQ are generally lower than adjacent organic-rich shale, but the pore throat radius are commonly greater. Compared with Type A shale, the pressurization caused by hydrocarbon generation and concentration of the adjacent shale is much greater due to greater HCGQ (Law and Dickinson 1985; Yurewicz et al., 2008), and the capillary force is much greater of the adjacent shale due to smaller porosity and pore throat radius (Wang

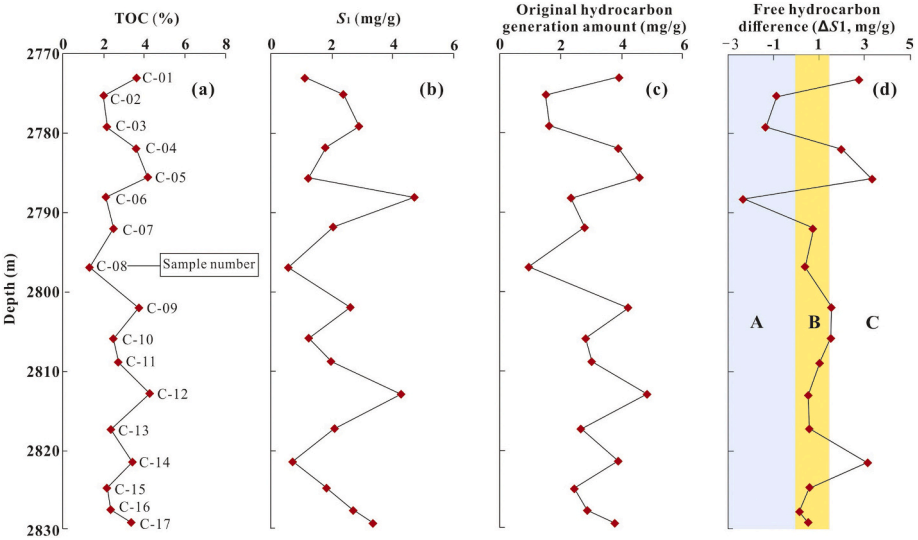

Fig. 8. Evaluation procedures for free hydrocarbon difference method (Li et al. 2016b, 2019a). (a) Correlation between TOC and depth; (b) Correlation between pyrolysis S_1 and depth; (c) Correlation between original hydrocarbon generation amount and depth; (d) Correlation between free hydrocarbon difference and depth.

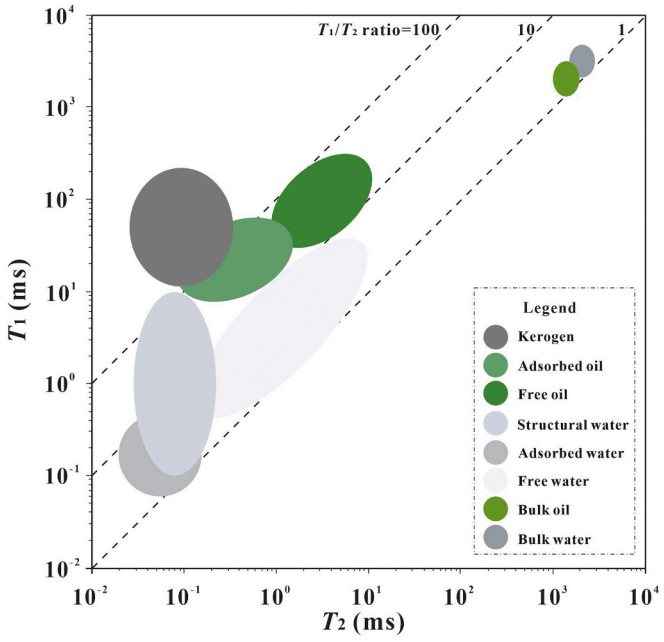

Fig. 9. Distribution characteristics of T_1-T_2 spectra for kerogen, kerogen with adsorbed oil, clay minerals with different water-containing states, shale, extracted shale, oil saturated shale, and water saturated shale (Wang et al. 2018c; Li et al. 2018b, 2020c).

et al. 2020). The differential overpressure (Osborne and Swarbrick 1997), capillary force, and hydrocarbon concentration promote the oil migration from adjacent to lean shales. The Type A unit is an open oil-rich unit with a high movable oil content. $\delta S_1 > 0$ or ≈ 0 indicates that the original HCGQ is equivalent to the existing free hydrocarbon amount, which is a poor connection with the adjacent shale and is a closed unit (Type B). Type B shale can be divided into two types: Shale with a high TOC content and a high HCGQ that is not discharged outward due to the relative isolation of the shale, resulting in a high free oil content, corresponding to a closed oil-rich unit (Type B_1). ② Shale with a low TOC content and a low HCGQ. Due to low original HCGQ and poor connectivity with the adjacent shales, the residual oil is limited, corresponding to a closed oil-poor unit (Type B_2). $\delta S_1 > 0$ (Type C) denotes that the original HCGQ is greater than the actual free hydrocarbon amount, indicating that the generated oil is mainly discharged to the outside. Type C shale has a high TOC content, large amount of oil, microfractures, and good connectivity with the adjacent strata, resulting in a large amount of oil expelled from the shale and a low oil content, corresponding to an open oil-poor unit. Regarding the movable oil content, type A > type B_1 > type B_2 > type C (Fig. 8) (Li et al. 2016b, 2019a).

However, this method has three limitations: It only provides a qualitative comparison of the oil content and fails to make an accurate quantitative evaluation. ② What the FHDM evaluates is whether the shale oil has micro-migration and if so, what the micro-migration intensity is. In analyzing oil migration, the shale thickness and internal stratigraphy should be further considered. The movable oil content is controlled not only by the hydrocarbon generation and expulsion capacity but also by the pore space and adsorption capacity of the shale (Lu et al. 2016; Feng et al. 2019; Li et al., 2014, Li et al., 2020a; Liu et al. 2020); ③ The hydrocarbon generation and expulsion stratigraphic units mentioned in the FHDM are not clearly defined. Rather than random selected cores, the stratigraphic units might be better defined by referring to the cores with different lithofacies.

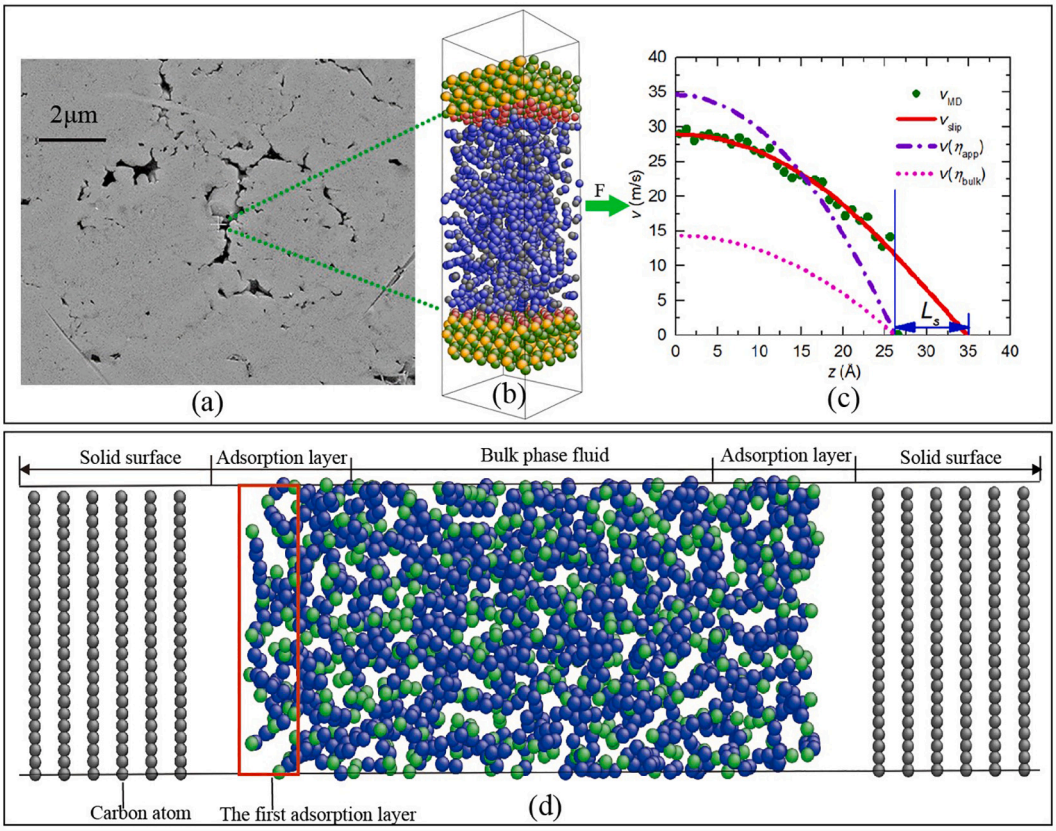

Fig. 10. Occurrence state and fluidity of the liquid alkane in shale pores by using molecular dynamics simulation (Wang et al. 2015b, Wang et al., 2016a, b, 2019b). (a) SEM image of an ion-milled Woodford chert sample; (b) Simulation snapshot of n-octane flow through a 7.8-nm quartz slit (perspective view); (c) Velocity profiles of n-octane in a 5.24-nm quartz nanopore; (d) Occurrence of n-heptane in pores and fissures of organic matter with a width of 7.8 nm.

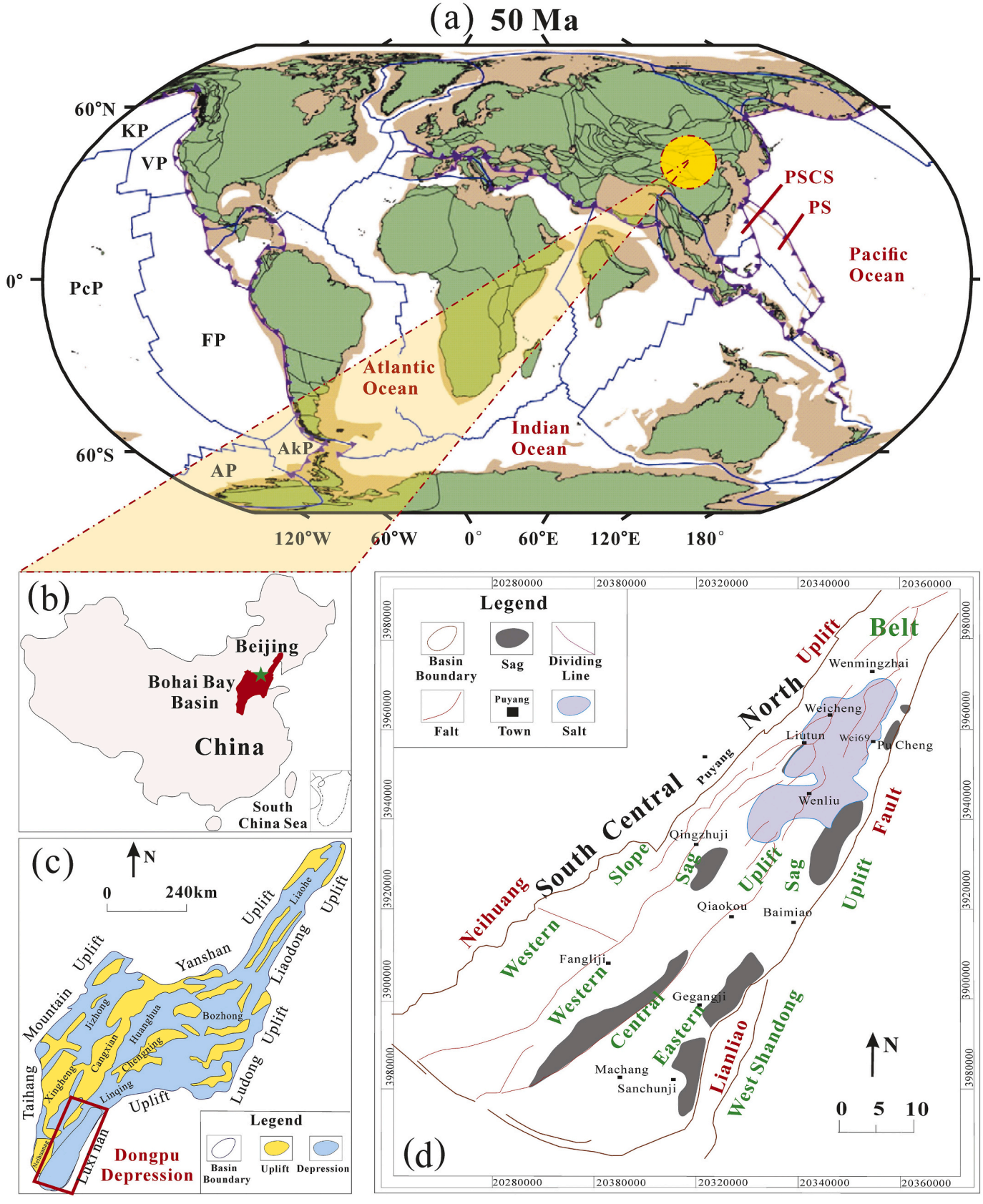

Fig. 11. (a) Tectonic location of the Bohai Bay Basin in 50 Ma on Earth (Matthews et al. 2016); (b) Overview map of China showing the location of Bohai Bay Basin; (c) Overview map of Bohai Bay Basin showing the location of Dongpu Depression (DD) (Tang et al. 2020); (d) Distribution of faults (middle of the third member of Shahejie Formation) and sags in the DD, modified after Wang et al. (2015a).

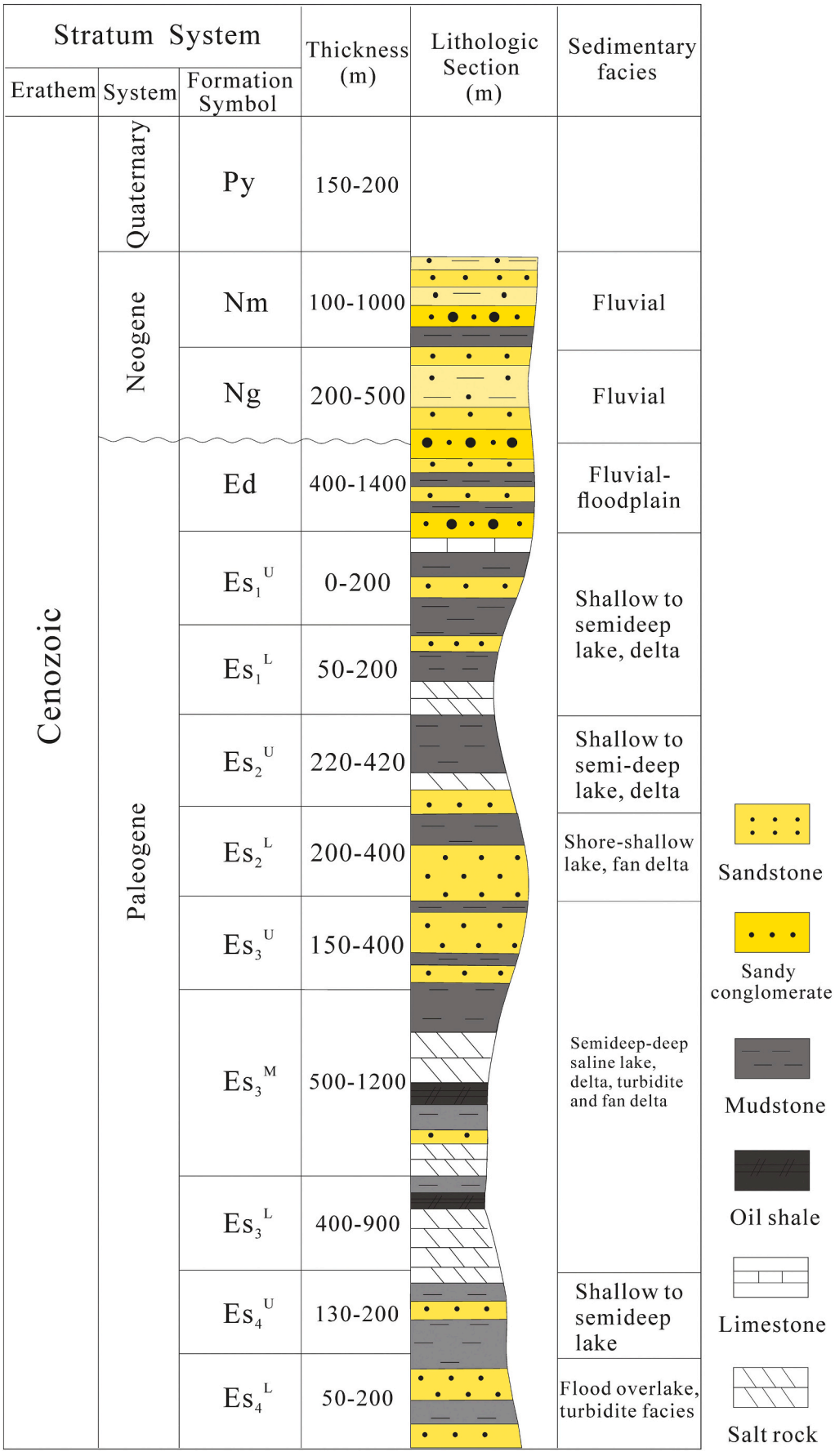

Fig. 12. Generalized Paleogene stratigraphy of the DD. Py: Pingyuan Formation; Nm: Minghuazhen Formation; Ng: Guantao Formation; E_3d: Dongying Formation; E_2s: Shahejie Formation; $E_2s_1^U$: Upper sub-member of first member of E_2s; $E_2s_1^L$: Lower sub-member of first member of E_2s; $E_2s_2^U$: Upper sub-member of second member of E_2s; $E_2s_2^L$: Lower sub-member of second member of E_2s; $E_2s_3^U$: Upper sub-member of third member of E_2s; $E_2s_3^M$: Middle sub-member of third member of E_2s_3; $E_2s_3^L$: Lower sub-member of third member of E_2s_3; $E_2s_4^U$: Upper sub-member of fourth member of E_2s; $E_2s_4^L$: Lower sub-member of fourth member of E_2s_4.

2.8. Swelling method (SM)

Swelling is a natural property of polymers and can cause the surrounding hydrocarbons to spontaneously absorb, which is a volumetric change (Sandvik et al. 1992). The swelling rate (the ratio of the volumes before and after swelling) is related to the volume and structure of the kerogen. Kerogen generally occupies a large volume in organic-rich shale, so swelling has a great influence on shale oil retention. For example, the swelling rate of the kerogen in the Green River and Rundle shales can be up to 3 (Larsen and Li, 1997). Therefore, surface effects of swelling and adsorption are two distinct mechanisms of oil retention. The adsorbed and swelling oil are immovable, and hence movable oil can be obtained by subtracting adsorbed and swelling oil contents from the total oil content (Li et al. 2016a).

Researchers have evaluated the adsorption-swelling oil amount of inorganic minerals and kerogen. During the evaluation, the samples were first soaked and saturated in oil, then centrifuged at 3000 RPM for 15 min, and then dried at 50 °C for 12 h; the oils that were not centrifuged and evaporated were considered immovable oils. Results showed that the adsorption/swelling amount of quartz on asphaltenes was approximately 4.5 mg HC/g rock (Ribeiro et al. 2009), the asphaltene adsorption from toluene on quartz was 6.4 mg HC/g rock (Pernyeszi et al. 1998), but that of powdered quartz to oil was only approximately 2 mg HC/g rock (Daughney 2000). For the Shahejie shales in the Dongying Depression, Bohai Bay Basin, the measured adsorption/swelling amount of quartz to oil were mainly 0.20–3.82 mg HC/g rock (Zhang et al. 2015; Li et al. 2016a). The measured adsorption/swelling amount of clay minerals on oil varied greatly, mainly ranging from 8.7–23.3 mg HC/g rock (Li et al. 2016a), whereas those of kaolinite and illite on asphaltenes reached 33.9 mg HC/g rock and 17.1 mg HC/g rock, respectively (Pernyeszi et al. 1998). The adsorption capacity of carbonate minerals to oil is weak. For example, the adsorption/swelling results of limestone and dolomite pieces on asphaltenes were 1.8 mg/m^2 and 1.6 mg/m^2, respectively (Yuan and Idris 1995), and that of powdered calcite on resin and asphaltene was 2.1–3.6 mg HC/g rock (Mohammadi and Sedighi 2013). Based on the above studies, Li et al. (2016a) established a conceptual model for adsorbed/swelling oil content evaluation (Eq. 3–5).

$$S_p = p_0 x_0 + \gamma \sum_{i=1}^{n} p_i x_i \tag{3}$$

Sp is the adsorbed/swelling oil content; p_0 and x_0 are the organic matter content and oil adsorption/swelling capacity, respectively; p_i and x_i are the content of mineral i and its oil adsorption/swelling capacity, respectively; γ is coefficient reflecting the change in SSA change.

$$p_0 + \sum_{i=1}^{n} p_i = 1 \tag{4}$$

Assuming pores are spherical, the SSAs before and after compaction are S_0 and S, respectively, and the SSA change coefficient can be expressed as Eq. 5 (Kieffer et al., 1999):

$$\gamma = \frac{S}{S_0} = \left[\frac{\varphi}{\varphi_0}\right]^{2/3} \tag{5}$$

φ and φ_0 are the present and original porosity, respectively.

However, the SM suffers four limitations: ① Test accuracy of shale porosity is affected by many factors. For example, Dean Stark extraction is necessary before porosity test, while some labile fraction of organic matter will be dissolved in this process, resulting in a porosity overestimation (Modiea and Lapierre 2012). ② Similar to the MREPM, there will be significant light hydrocarbon losses in the process of sample preservation and preparation (Espitalié et al. 1977; Lafargue et al., 1998; Behar et al. 2001; Michael et al. 2013). ③ Application of this method requires a large number of experimental parameters, such as those of different minerals and kerogens with different maturities, the porosity and the SSA. Similar to the MSEM, the analysis process of SM is complex, complicated and expensive and therefore limited to samples. ④ The solvent extraction cannot complete the selective separation of the adsorbed and swelling oil, and the change in solvent and extraction methods may cause experimental data variation.

2.9. Nuclear magnetic resonance (NMR)

NMR technology is noninvasive and nondestructive to pore structures of shale and is sensitive to fluids (Williams et al. 1991). However, due to the existence of irreducible and movable oil in an arbitrary pore space of shale, each pore (relaxation time) contains a contribution of irreducible fluid, and the corresponding pore contains different amounts of irreducible oil with different relaxation times. Therefore, the combination of NMR and centrifugal/displacement analyses is much more widely applied. The principle of this combination is to conduct NMR analysis of a shale core before and after centrifugation/displacement and evaluate the movable oil content and distribution by NMR T_2 spectra (Karimi et al. 2015; Dang et al. 2018; Zhou et al. 2016). However, because shale features various hydrogen-containing components, such as kerogen, bitumen, oil and water, and the T_2 spectra provide only limited information (Fleury and Romero-Sarmiento, 2016; Mehana and El-monier, 2016; Li et al. 2018b), two-dimensional T_1-T_2 spectra are increasingly used in movable oil evaluation. However, this method mainly focuses on kerogen and oil-bearing property evaluation and is rarely used in oil content evaluation (Birdwell and Washburn 2015; Kausik et al. 2017; Li et al. 2018b, 2020c). Wang et al. (2018c) and Li et al. (2018b) used NMR to analyze the distribution characteristics of T_1-T_2 spectra for kerogen, kerogen with adsorbed oil, clay minerals with different water-containing states, shale, extracted shale, oil saturated shale, and water saturated shale and summarized their distribution in T_1-T_2 spectra. Li et al. (2020c) subsequently improved the distribution pattern of T_1-T_2 spectra (Fig. 9), making it possible to evaluate oil with different occurrence states.

This method suffers four limitations. ① It is effective in conventional reservoirs, but the displacement/centrifugation is less efficient for tight shale. In addition, excessive pressure might cause artificial fractures and subsequently affect experimental results (Li et al., 2019b). ② During centrifugation or displacement, one problem is that how much oil expelled at a certain centrifugal rate or how much displacement pressure corresponds to the movable oil is unclear. ③ When the pore throat of shale is small enough, the physical implication of NMR parameters may change (Lu et al. 2016). ④ The analyses of centrifugation/displacement and NMR are complex, complicated, and expensive and limited to representative samples.

2.10. Molecular dynamics simulation (MDS)

MDS mainly utilizes Newtonian mechanics to simulate motion trajectory of molecules and calculates structure and properties of the system by performing statistical averaging through an ensemble composed of different states (Jorgensen et al. 1984; Plimpton 1995; Ambrose et al. 2012). Researchers have tried to use MDS to analyze occurrence state and fluidity of liquid alkane in shale pores (Wang et al. 2015b, Wang et al., 2016a, Wang et al., 2016b, Wang et al., 2019b; Tian et al. 2017; Li et al. 2019b) (Fig. 10). Although the MDS has implications for understanding microscale occurrence mechanism of shale oil, its application is still limited, mainly due to the following three reasons: ① It is difficult to fully consider heterogeneity of pore and fracture systems in shales by using only narrow fractures during simulation. ② The accuracy of this method depends on force field model selection, but the force field applicable to different substances are not the same (Jorgensen et al. 1984; Ambrose et al. 2012). ③ During simulation, graphene is generally used to represent organic matter structure, and the six layers of graphene are used as the solid surface of the nanopores of organic matter, but both of which are far from sufficient for describing the heterogeneity

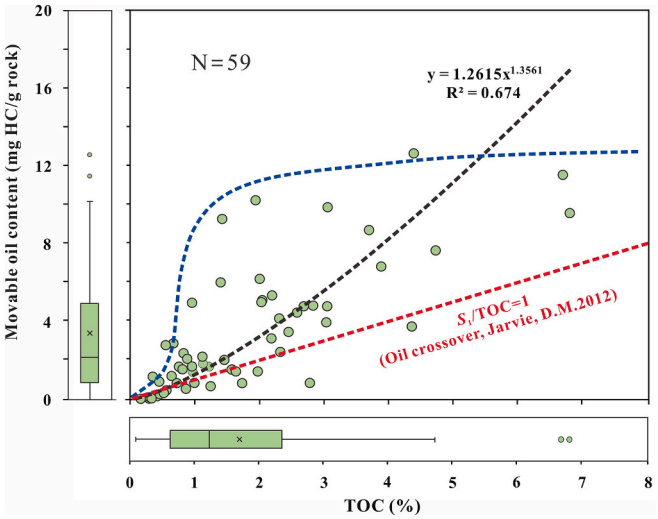

Fig. 13. Correlations between TOC contents and movable oil contents (S_{11} + S_{21}) of the Paleogene shales in the Dongpu Depression. N indicates the number of samples.

of kerogen (Ambrose et al. 2012; Harrison et al. 2014).

In view of the above methods, this study utilizes the well-developed MREPM to evaluate oil content parameters, and these parameters are calibrated for light hydrocarbons to evaluate movable oil content.

3. Geological framework of the DD

The Bohai Bay Basin is a well-known petroliferous basin in eastern China (Fig. 11a and b). The thick shale in the Paleogene Shahejie Fm. (50.5–33 Ma) is the most important source rock in the Bohai Bay Basin, with a thickness that is generally 500–600 m, but can reach 2000–3000 m (Jin 2001; Zou et al. 2019). The DD, located in the Linqing Depression of the southeast corner of the Bohai Bay Basin (Fig. 11c), is a Cenozoic lacustrine rift basin on Paleozoic and Mesozoic basement, with a north-northeast strike and an area of 5.3 × 10^3 km^2. The DD is wide in the north and narrow in the south, bounded by the Luxi uplift to the east and the Lankao uplift to the south and the Shenxian Sag to the north and overlying the Neihuang uplift in the west. The DD is mainly composed of the western slope zone, western sag zone, central uplift zone, eastern depression zone, and eastern steep slope zone (Fig. 11d) (Wang et al. 2015a). The Shahejie Fm. (Es) developed the fourth (Es_4), third (Es_3), second (Es_2), and first (Es_1) members (Fig. 12), with a total thickness of approximately 4800 m. The shale mainly developed in the lower section of Es_4 and middle - upper section of Es_3, with a cumulative thickness of 2750 m (Wu et al. 2003). The shale is mainly composed of semideep lacustrine and deep lacustrine deposits, mainly feldspathic, carbonate, and mixed fine-grained sedimentary rocks, including brown-gray shale, gray-dark gray calcareous shale, dolomitic shale, and dark gray-gray gypsum mudstone (Zhang et al. 2015), which provide a strong matrix to host shale oil resources (Wang et al. 2015a; Zhang et al. 2015; Li et al. 2020a).

4. Samples and methods

4.1. Sample selection

Fifty-nine shale core samples from nine exploration wells with different textures (massive, layered, and laminar), color (black, gray, brown and light green), and mineral composition were tested in this study.

4.2. Experimental tests

A CS-230HC carbon and sulfur analyzer was used to measure TOC. First, the shale cores were crushed to 80–100 mesh, and the carbonate minerals were removed with dilute hydrochloric acid. The carbonate minerals were completely reacted in a water bath or by heating, then the sample was washed with distilled water. The samples were placed in a dryer for 7 h, and iron and nickel combustibles were added into the crucible. The samples were put into a sampler, and the experimental results were obtained after combustion in a high-temperature oxygen flow. The MREPM was conducted using a Rock-Eval 6 apparatus at the Wuxi Institute of Petroleum Geology, SINOPEC. First, a sample was heated to 200 °C, and this temperature was maintained for 1 min to obtain S_{11}; then, the sample was heated to 350 °C, 450 °C, and 600 °C at 25 °C/min to test S_{21}, S_{22} and S_{23}, which are the light-medium oil components in free state, heavy asphaltene components, and kerogen pyrolysis hydrocarbons, respectively. (S_{11}+ S_{21}) is the movable oil content of shale (Jiang et al. 2016). XRD was performed with a Brucker D8 Focus to analyze minerals. The samples were first crushed to approximately 300 mesh. Whole rock fragments were prepared by the back-pressure method, and a whole rock slice was put into the XRD apparatus (Kamp 2008).

A high-pressure mercury injection analysis was conducted using a Poremaster GT60 mercury injection instrument. The experimental procedure was consistent with Chen et al. (2017). A nitrogen isothermal adsorption experiment was conducted with an AutoSorb IQ automatic SSA and pore diameter analyzer. Before the test, samples were pretreated by vacuum degassing, for which the temperature was set to 110 °C and maintained for 8 h. Then, the nitrogen adsorption capacity of samples per unit mass under different relative pressures was measured by gradually increasing the pressure. When the system pressure reaches the saturated vapor pressure, that is, P_0 = 0.101 MPa, the system pressure is gradually reduced to measure the desorption volume of nitrogen under different relative pressures. Consistent with Chen et al. (2017), the SSA was calculated using the Brunauer-Emmett-Teller (BET) equation, and the pore size distribution was calculated using the Barrett-Joyner-Halenda (BJH) method. The instrument used in the CO_2 adsorption experiment was the same as that used in the nitrogen adsorption experiment. First, the sample adsorbed by nitrogen was degassed to remove nitrogen adsorbed on the surface and inside of the sample. Then, CO_2 was injected at a low temperature of 0 °C. In this case, CO_2 entered pores as small as 0.3 nm to obtain a series of pressure and CO_2 adsorption data. Finally, pore volume and SSA of the micropores were calculated based on the density functional theory (DFT) theoretical density model of molecular statistical thermodynamics.

4.3. Light hydrocarbon calibration

In this study, the MREPM was used to quantitatively characterize movable oil content. However, shale cores undergo significant changes when moved from underground to surface conditions. In addition, during core preservation and sample preparation, significant light hydrocarbon loss occurs (Espitalié et al. 1977; Lafargue et al., 1998; Behar et al. 2001). Notably, the lost light hydrocarbons are very important to quantify for shale oil exploitation (Zhu et al. 2015; Lu et al. 2016; Xue et al. 2016), it is necessary to determine the light hydrocarbon loss. The DD and Dongying Depression are two adjacent lacustrine rift basins in Bohai Bay Basin. During the Paleocene-Eocene period, the shales of both areas developed in brackish-saline lakes. The organic matter of this shale was mainly derived from lower aquatic organisms, and the main types of organic matter in this shale are Type I and II_1 (Zhu and Jing, 2003; Zhu et al. 2015; Hu et al. 2018b; Tang et al. 2020). Therefore, this study used the light hydrocarbon calibration coefficient standard of pyrolysis S_1 of the Es Fm. shale in the Dongying Depression (Zhu et al. 2015). The standard was established as follows: Cores were selected at drilling coring site and were sealed and frozen simultaneously. ② The well

mixed samples were divided into 2 groups. The first group was grounded and pyrolysis analyses were performed under frozen conditions by liquid nitrogen. Because it usually takes more than 30 days for ordinary cores to be moved from the well site to the core store for storage, the second group was grounded left at room temperature for 30 days, and then pyrolysis analyses were performed at room temperature. ③ The difference in pyrolysis ($S_1 + S_2$) values between two groups is the lost light hydrocarbon ($\Delta(S_1 + S_2)$). The ratio of $\Delta(S_1 + S_2)$ to ($S_1 + S_2$) is the light hydrocarbon calibration coefficient (Zhu et al. 2015).

5. Results

5.1. Movable oil content

By combining MREPM and light hydrocarbon calibration, corrected movable oil contents ($S_{11} + S_{21}$) were obtained. The results show that the ($S_{11} + S_{21}$) of the shale is ranges from 0.031–12.64 mg HC/g rock, with an average of 3.39 mg HC/g rock. Further calculation of the OSI (($S_{11} + S_{21}$)/TOC × 100) shows that the values range from 14.9–651.8 mg HC/g TOC, with a mean of 187.8 mg HC/g TOC. Approximately 71.2% of the shale samples have OSI values greater than 100 mg HC/g TOC, indicating that the shale in the DD has potential for shale oil yields (Fig. 13). For example, a large amount of bitumen is developed in the shale in the study area, and part of it has weak orange yellow fluorescence (Fig. 14).

5.2. Organic matter richness

TOC content and oil generation potential ($S_1 + S_2$) are important indices for evaluating organic matter richness of shale. In detail, with

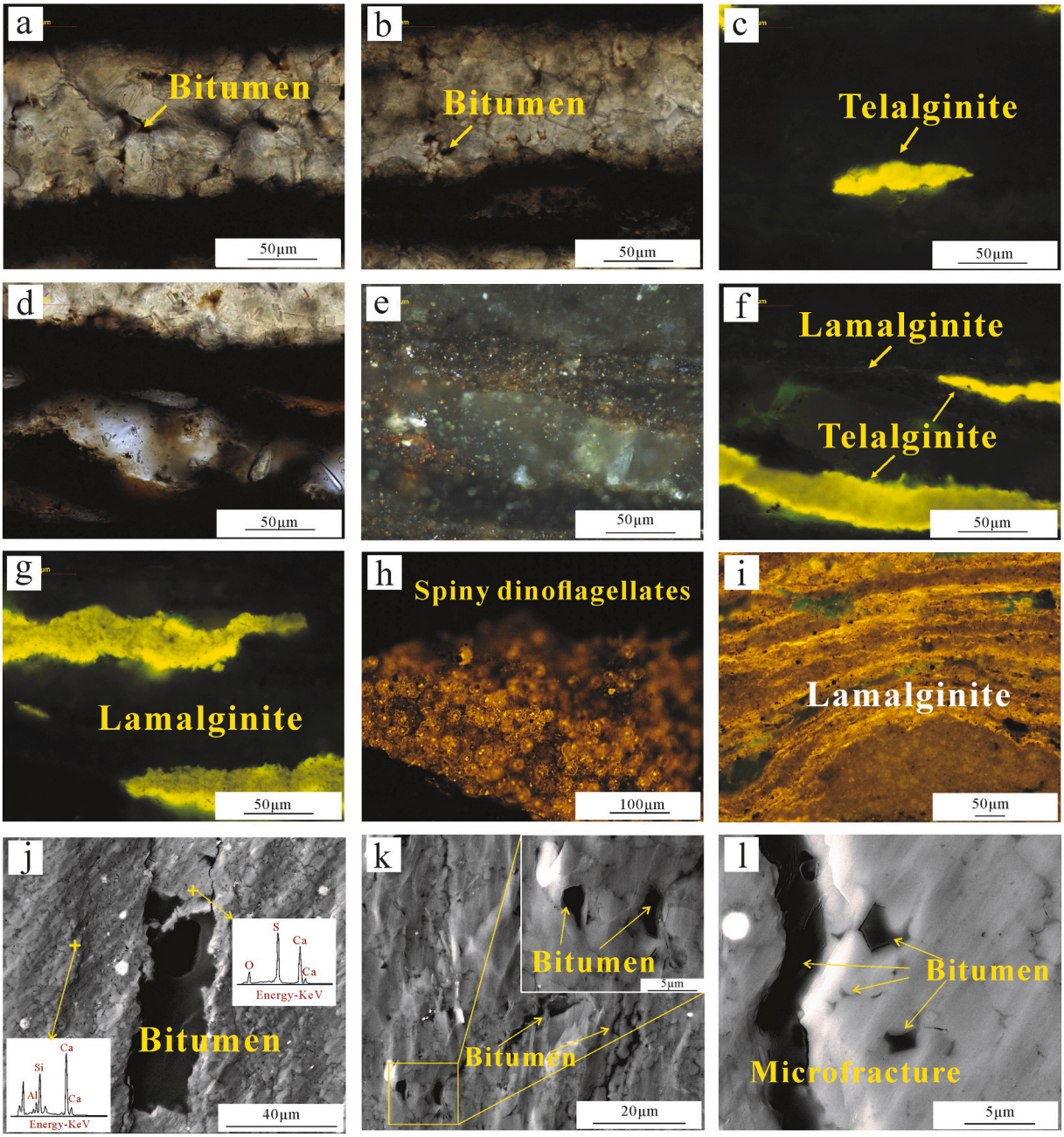

Fig. 14. Microscopic and FE-SEM images of oil-generating biota in Paleogene shales of the DD. (a)-(g) Well Wen 248, 3365.7 m; (h) Well Wen 248, 3353 m; (i) Well Wei 79–13, 3370.28 m; (j) Well Wei 20, 2641.57 m; (k) Well Wei 42, 3461.65 m; (l) Well Wen 210, 3848.2 m. ((j)-(l) were cited from Shao et al. 2018).

similar kerogen type and thermal maturity, shales with TOC contents of less than 0.5%, 0.5–1%, 1–2%, 2–4%, and greater than 4% represent poor, fair, good, very good, and excellent petroleum potential respectively (Peters and Cassa 1994). The shales with poor-fair petroleum potential are non-source rocks. The shales with ($S_1 + S_2$) values of less than 3, 3–6, 6–12, 12–24, and greater than 24 mg HC/g rock represent poor, fair, good, very good, and excellent petroleum potential respectively (Peters and Cassa 1994). The test results of 59 samples show that the TOC contents are 0.10%–6.78%, with an average of 1.77%. Combining the data obtained by the MREPM and light hydrocarbon calibration, results show that the ($S_{11} + S_{21} + S_{22} + S_{23}$) is 0.14–47.59 mg HC/g rock, with a mean of 9.49 mg HC/g rock (Fig. 15). In terms of TOC contents, the shales with poor, fair, good, very good, and excellent petroleum potential account for 16.9%, 25.4%, 22.0%, 27.1%, and 8.5%, respectively (Table 2); thus, 57.6% of the tested samples represent good petroleum potential from the perspective of TOC. From the perspective of ($S_{11} + S_{21} + S_{22} + S_{23}$), the shales with poor, fair, good, very good, and excellent petroleum potential account for 30.5%, 20.3%, 15.3%, 27.1%, and 6.8% respectively (Table 2), of which 49.2% represent good petroleum potential. The proportions of shales with different petroleum potential evaluated by the two indices are different, this is related to the differences in the evaluation criteria. Overall, the shale in the DD largely represents good petroleum potential.

5.3. Organic matter type

The relationship between pyrolysis T_{max} and hydrogen index (HI) is commonly used for organic matter type evaluation (Espitalié 1982). The test results of 59 samples show that the *T*max ranges from 404 to 495 °C, with an average of 440.5 °C, whereas the HI ranges from 7.1–651 mg/g, with a mean of 271.3 mg/g. The results show that kerogen types I (sapropelic), II_1 (humic-sapropelic), II_2 (sapropelic-humic), and III (humic) account for 14.5%, 46.8%, 29.0%, and 6.5% of these shale samples, respectively (Fig. 16; Table 2), indicating that the organic matter types are mainly Type II and Type I, and that Type II_1 is the most abundant type. Microscopic observation results of the hydrocarbon-generation biota show that the organic matter of the shale is mainly amorphous, layered alginite, telalginite and solid bitumen. The amorphous organic matter mainly is derived from cyanobacteria. The lamellar alginite is distributed in argillaceous laminae with yellow-green fluorescence. The telalginite is brownish-yellow under transmitted light, with bright yellow fluorescence (Fig. 14c and f). Generally, organic matter originating from low aquatic algae is mainly Type I and Type II_1. This is consistent with the results obtained by the T_{max} - HI plot. Therefore, the shale in the DD is dominated by oil-prone kerogen with a strong oil generation ability.

5.4. Thermal maturity

Pyrolysis T_{max} is commonly used to evaluate the thermal maturity of shale, and the *T*max values of less than 435 °C, 435–445 °C, 445–450 °C, 450–470 °C, and greater than 470 °C represent the immature, early mature, peak mature, late mature, and post mature stages, respectively (Peters and Cassa 1994). Whereas the bitumen or oil/water-based mud additives "contamination" of kerogen and neglection of analytical uncertainties or natural variability within a stratigraphic unit at any given locality may cause T_{max} suppression (Clementz 1979; Lafargue et al., 1998; Katz and Lin 2020), which might bias thermal maturity of shales. By splitting the standard S_2 peak into S_{2-1} (adsorbed heavy oil and swelling oil) and S_{2-2} (kerogen cracked hydrocarbons) peaks using MREPM, the T_{max} anomaly caused by "contamination" was avoided. The test results show that *T*max ranges from 404 to 495 °C, with a mean of 440.5 °C. Immature, early mature, peak mature, late mature, and post mature shale account for 22.6%, 41.9%, and 19.4%, 12.9%, and 3.2%, respectively. Therefore, 96.8% of the shale samples are in immature-mature stages (Fig. 16; Table 2), which is conducive to shale oil enrichment.

5.5. Mineralogy

XRD results show that the shale has a high clay mineral content, ranging from 0 to 62.7%, with an average of 32.8%. The contents of calcite, quartz, dolomite, ankerite, and feldspar range from 0%–62.3%, 1.1%–36%, 0%–96.9%, 0%–55.6%, and 1.3%–28.1%, with averages of 17.4%, 14.1%, 13.3%, 9.0%, and 7.0%, respectively. The shale also contains some pyrite and gypsum, and the contents are 0%–8.9% and 0%–8.1%, with averages of 2.0% and 1.8%, respectively (Fig. 17). Overall, the mineral composition of the shale in the DD is complex, which is related to the strong heterogeneity of lacustrine sediments. Shale minerals can be divided into felsic, clay and carbonate minerals. The felsic minerals mainly include quartz and feldspar, and the carbonate minerals mainly include calcite, dolomite and ankerite. In comparison, the mineral compositions of these 59 shale samples in the DD are similar, mainly carbonate and clay minerals. Among them, the content of carbonate is the highest, ranging from 0 to 96.9% with a mean of 40.2%. This is followed by clay minerals, with a content ranging from 0%–62.7%, with an average of 32.8%. The felsic mineral content is the lowest, ranging from 3.1%–53.3%, with an average of 21.0% (Fig. 17).

5.6. Pore volume

Shale has abundant micro−/nanoscale pores (Loucks et al. 2012; Zou et al. 2013, 2019). Results of isothermal adsorption-desorption experiments of the 59 samples show that although the shapes of the adsorption-desorption isotherms and the gas adsorption capacity vary, the isotherms feature an inverse-S shaped hysteresis loop (Fig. 18). Specifically, when the relative pressure (P/P_0) is less than 0.05, the nitrogen adsorption isotherm appears as a slight upward bulge, corresponding to the adsorption of nitrogen molecules on the shale surface. When P/P_0 is 0.05–0.45, the adsorption isotherm rises approximately linearly, which mainly corresponds to multi-molecular layer adsorption of nitrogen molecules on the shale surface. When P/P_0 is greater than 0.45, the adsorption isotherm shape bends downward with increasing P/P_0. In addition, when P/P_0 is close to 1.0, the adsorption capacity still rises rapidly, and there is no adsorption saturation, indicating that the shale in the DD mainly develops macropores (greater than 50 nm) and mesopores (2–50 nm). Generally, as P/P_0 is greater than 0.45, all the adsorption and desorption isotherms start to separate, forming the

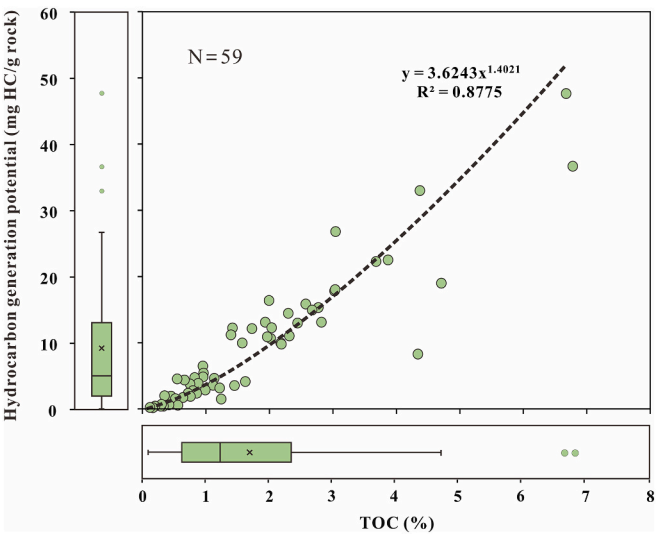

Fig. 15. Correlations between TOC contents and hydrocarbon generation potential ($S_1 + S_2$) of the Paleogene shales in the Dongpu Depression. N indicates the number of samples.

Table 2
Experimental data for Paleogene shales in Dongpu Depression, Bohai Bay Basin.

Smaple NO.	Depth (m)	TOC (%)	Tmax (°C)	(S11 + S21) (mg/g)	Light hydrocarbon calibration coefficient	Calibrated (S11 + S21) (mg/g)	Calibrated OSI (mg/g)	(S22 + S23) (mg/g)	HI (mg/g)	TR	Original HI (mg/g)	Hydrocarbon expulsion amount (mg/g)	Kerogen type	Total pore volume (cm^3/g)	Totail SSA (m^2/g)	Clay mineral (%)	Felsic (%)	Carbonate (%)	Quartz (%)
1	3674.78	0.88	453	1.22	0.71	2.08	236.32	1.76	199.95	48.1	385.4	185.48	I	0.017	9.892	27.9	16.3	53.5	11.7
2	3411.65	1.97	452	1.1	0.30	1.43	72.70	9.41	477.66	44.3	857.8	380.11	I	0.014	9.589	34.7	18.2	38.7	11.3
3	3357.5	1.57	441	1.26	0.23	1.56	98.85	8.35	530.50	6.9	569.7	39.17	I	0.046	6.648	28.6	17.3	50.3	12.8
4	2730.75	1.73	436	0.76	0.10	0.83	48.26	11.26	651.24	1.0	657.6	6.32	I	0.015	6.942	25.1	15.8	51.8	11.9
5	3345.31	2.68	451	3.87	0.23	4.78	178.52	10.13	378.41	40.4	635.1	256.72	I	0.053	5.281	33.6	19.2	44.3	16.4
6	3687.46	2.03	452	2.93	0.71	5.00	246.70	5.60	276.54	44.3	496.6	220.06	I	0.026	9.107	16.9	15.6	62.3	8.4
7	3558.16	6.67	440	7.32	0.58	11.54	172.99	36.05	540.24	5.0	568.9	28.68	I	0.013	9.107	30.2	16.4	45.2	12.6
8	3557.58	3.05	436	6.26	0.58	9.87	323.99	16.88	553.99	1.0	559.4	5.37	I	0.045	4.968	26.3	10.9	60.1	9
9	3547.62	2.77	444	0.55	0.54	0.84	30.45	14.44	520.74	14.5	609.2	88.50	I	0.006	11.211	51.9	28.3	12.4	23.5
10	3431.1	1.22	451	1.27	0.32	1.68	137.82	1.45	119.05	63.9	329.8	210.75	II1	0.011	9.912	47.8	15.9	30.9	13.1
11	3556.88	4.38	437	8.23	0.54	12.64	288.83	20.31	464.23	3.0	478.4	14.15	II1	0.101	2.349	52.4	22	16.4	18.4
12	4156.23	0.95	451	2.25	1.21	4.96	520.16	1.48	155.17	63.9	429.9	274.70	II1	0.024	5.949	13.7	17.2	68	7.2
13	3184.9	0.96	435	1.25	0.14	1.43	148.17	3.95	409.41	0.9	413.0	3.56	II1	0.006	2.247	9.1	4.1	81.6	1.4
14	3365.7	2.82	448	3.85	0.25	4.82	170.76	8.24	292.10	50.0	584.4	292.28	II1	0.028	5.276	15.9	14.1	67.7	8.3
15	3212.03	0.52	447	0.29	0.15	0.33	64.38	1.20	231.39	44.8	419.6	188.18	II1	0.024	18.301	32.3	17.2	44.2	13.4
16	3404.1	0.96	445	1.3	0.30	1.69	177.01	3.12	326.29	34.1	495.3	169.04	II1	0.018	7.933	25.1	10.9	55.1	6.4
17	3274.2	0.86	443	0.46	0.18	0.54	62.98	1.88	218.15	23.6	285.6	67.44	II1	0.014	12.170	39.1	21.1	37.2	15.7
18	3362.6	1.13	447	1.47	0.25	1.84	163.20	2.80	248.45	44.8	450.5	202.04	II1	0.019	8.047	18.9	14.1	63.4	8.4
19	3559.65	1.40	438	3.81	0.58	6.01	429.78	5.14	367.67	4.8	386.3	18.63	II1	0.020	1.771	36.1	10.1	51.8	7.9
20	3356.75	3.68	445	7.04	0.23	8.69	235.97	13.54	367.54	34.1	557.9	190.41	II1	0.017	6.616	36.2	20.3	39.9	17.2
21	3677.81	2.19	449	3.13	0.71	5.34	243.68	4.40	200.91	54.9	445.9	245.01	II1	0.040	5.612	26.1	15	55.7	9.5
22	3188.8	2.32	439	2.13	0.14	2.44	105.18	8.56	369.60	7.3	398.9	29.27	II1	0.060	27.057	35.1	17.1	40.2	12
23	3167.22	6.78	435	8.44	0.14	9.58	141.30	27.03	398.67	0.9	402.1	3.47	II1	0.049	11.288	22.3	17.2	51.1	9.6
24	3155.12	2.58	436	3.93	0.14	4.46	173.24	11.34	440.39	1.7	447.9	7.50	II1	0.047	16.430	27.9	16	49.7	11
25	3263.42	2.18	447	2.65	0.18	3.13	143.35	6.78	310.87	44.8	563.7	252.81	II1	0.051	21.656	40.5	17.2	39	12.7
26	3282.66	2.45	438	2.92	0.19	3.47	141.83	9.47	387.32	4.8	406.9	19.62	II1	0.060	20.728	35.9	17.8	35.3	11.1
27	3278.1	3.04	440	4.05	0.18	4.78	157.23	13.21	434.68	10.5	485.8	51.16	II1	0.032	8.846	25.1	16.1	53.6	7.6
28	3467.8	0.72	447	0.61	0.38	0.84	116.76	1.47	204.45	44.8	370.7	166.27	II1	0.007	9.156	41.6	21	28.5	14
29	3685.7	1.12	450	1.29	0.71	2.20	197.26	1.32	118.39	59.6	292.9	174.54	II1	0.047	11.366	39.6	28.5	14.8	21.2
30	3271.38	2.00	437	5.24	0.18	6.18	309.42	10.17	509.01	3.0	524.5	15.51	II1	0.060	21.539	33	21.8	23.5	15.7
31	3192.5	2.30	437	3.64	0.14	4.16	181.07	10.23	444.98	3.0	458.5	13.56	II1	0.075	33.683	62.7	22.2	10.5	16.7
32	3190.75	3.87	435	5.97	0.14	6.83	176.29	15.65	404.08	0.9	407.6	3.52	II1	0.063	20.451	40.9	22.5	31.3	14.1
33	3178	3.03	438	3.46	0.14	3.96	130.72	13.83	456.89	4.8	480.0	23.15	II1	0.076	26.656	37.6	20.3	26	13.9
34	3376.37	0.55	438	2.23	0.25	2.79	507.77	1.70	309.37	4.8	325.0	15.67	II1	0.020	4.956	21.9	52.7	22.7	36
35	3428.76	0.35	441	0.88	0.32	1.16	332.91	0.80	228.96	14.4	267.4	38.41	II1	0.027	4.128	13.5	5.9	80.6	4.6
36	4154.03	1.94	448	4.65	1.20	10.23	528.41	2.83	146.18	50.0	292.4	146.27	II1	0.023	8.350	17.6	10.7	68.8	7
37	3284.65	2.04	433	4.29	0.19	5.10	249.83	7.12	349.02	0.2	349.6	0.57	II1	0.051	11.966	38.8	24.3	31.6	5.7
38	3447.1	0.30	447	0.08	0.35	0.11	35.80	0.55	182.66	44.8	331.2	148.55	II1	0.015	20.854	43.3	21	31.7	17.5
39	3383	0.67	431	2.21	0.30	2.88	431.58	1.46	219.15	16.0	260.7	41.59	II2	0.024	4.948	25.3	10.7	62.6	9
40	3688.2	1.24	456	0.4	0.71	0.68	54.82	0.76	61.09	77.3	269.2	208.13	II2	0.015	9.362	13.1	40.7	28.5	28
41	3279.2	4.71	433	6.44	0.19	7.65	162.31	11.30	239.81	21.0	303.4	63.63	II2	0.049	8.680	39.2	45.6	0	17.5
42	3416.58	0.75	436	1.27	0.32	1.68	222.96	2.04	270.95	29.3	383.2	112.20	II2	0.010	5.333	23.9	8.7	66	7.1
43	3159.12	0.46	432	0.23	0.14	0.26	57.00	0.85	185.59	18.4	227.4	41.83	II2	0.003	1.092	0	3.1	96.9	1.6
44	3385.32	4.34	447	5.12	0.30	6.66	153.34	4.49	103.36	59.7	256.6	153.25	II2	0.052	16.361	15.4	13.6	66.1	7
45	3420.1	0.45	438	0.69	0.32	0.91	202.13	0.97	214.98	35.1	331.2	116.25	II2	0.021	10.117	28.4	10.9	60.7	8.5
46	3383.85	0.83	424	1.82	0.30	2.37	287.01	2.33	282.42	3.9	293.8	11.42	II2	0.031	5.331	27.4	13.6	50.5	10.2
47	4155.2	1.42	424	4.21	1.20	9.26	651.79	2.94	206.90	3.9	215.3	8.37	II2	0.026	6.689	21	11.3	64.3	9.1
48	3452.9	0.42	445	0.12	0.38	0.17	39.40	0.41	97.83	54.7	216.1	118.30	II2	0.015	19.884	41.7	28.2	25.2	19.3
49	3532.81	0.33	436	0.04	0.45	0.06	17.40	0.33	99.31	29.3	140.4	41.12	II2	0.031	29.394	60.2	31.3	6.9	24.1
50	3563.05	0.80	432	0.98	0.58	1.55	193.64	1.17	146.60	18.4	179.6	33.04	II2	0.017	9.373	42.5	16.1	28.9	13.4
51	3523.07	0.29	441	0.03	0.45	0.04	14.90	0.33	113.36	43.8	201.7	88.36	II2	0.023	26.110	51.6	26.2	21.5	21.1

(*continued on next page*)

Table 2 (*continued*)

Smaple NO.	Depth (m)	TOC (%)	Tmax (°C)	(S11 + S21) (mg/g)	Light hydrocarbon calibration coefficient	Calibrated (S11 + S21) (mg/g)	Calibrated OSI (mg/g)	(S22 + S23) (mg/g)	HI (mg/g)	TR	Original HI (mg/g)	Hydrocarbon expulsion amount (mg/g)	Kerogen type	Total pore volume (cm^3/g)	Totail SSA (m^2/g)	Clay mineral (%)	Felsic (%)	Carbonate (%)	Quartz (%)
52	3285.55	1.63	435	1.21	0.19	1.44	88.46	2.66	163.69	26.4	222.5	58.83	II2	0.023	4.151	40.1	26.4	24.5	7.7
53	3420.9	0.99	434	0.64	0.32	0.85	85.32	1.98	199.68	23.7	261.6	61.88	II2	0.026	8.016	50.2	47.6	0	25.5
54	3182	1.45	413	1.77	0.14	2.02	139.22	1.47	101.10	7.0	108.7	7.61	III	0.031	3.995	15.7	21	43.4	1.1
55	3558.38	0.64	424	0.76	0.58	1.20	187.24	0.50	78.11	45.0	142.0	63.91	III	0.046	14.723	59.2	27	12.7	21.2
56	4152.44	0.56	404	0.21	1.20	0.46	82.37	0.04	7.13	2.0	7.3	0.15	III	0.072	26.740	50.2	31.6	9.1	26.9
57	3552.28	0.17	431	0.02	0.54	0.03	18.59	0.11	66.63	60.0	166.6	99.94	III	0.038	7.241	38.7	53.3	0	33.7
58	4178.29	0.10	495	0.1	1.21	0.22	223.69	0.14	141.96	1.9	144.7	2.75	–	0.023	19.148	44.1	41.6	14.4	32
59	4168.67	0.23	486	0.09	1.21	0.20	86.43	0.06	26.12	1.9	26.6	0.51	–	0.018	13.916	41.8	38.7	19.5	30.3

obvious inversed-S shaped hysteresis loop (Fig. 18). Meanwhile, the adsorption capacity of the desorption curve is clearly larger than that of the adsorption curve under the same P/P_0. According to the hysteresis loop types classified by the IUPAC (Fig. 19), the shales in the DD is mainly type H3 with a small amount of type H4, indicating that the shales mainly develop slit-shaped pores with a small amount of narrow slit-like pores.

By utilizing high-pressure mercury injection and nitrogen and CO_2 isothermal adsorption experiments, this study quantitatively characterized the pore volumes of shale macropores, mesopores, and micropores. The results show that the macropore volume is 0.1–97 $\times$ 10^{-3} cm^3/g, with an average of 16 $\times$ 10^{-3} cm^3/g; the mesopore volume is 1.6–49 $\times$ 10^{-3} cm^3/g, with a mean of 14 $\times$ 10^{-3} cm^3/g; and the micropore volume is 0.23–7.1 $\times$ 10^{-3} cm^3/g, with an average of 2.2 $\times$ 10^{-3} cm^3/g. This indicates that the pores within shales are mainly macropores and mesopores, which is conducive for movable oil enrichment (Zhu et al., 2019b; Liu et al. 2020). In general, the total pore volume of shale ranges from 2.8–100.6 $\times$ 10^{-3} cm^3/g, with an average of 32.5 $\times$ 10^{-3} cm^3/g.

5.7. SSA

Clay minerals and pores are key contributors to the SSA of shale (Kuila et al. 2014; Liu and Peng, 2017; Feng et al. 2019). The SSAs of macropores, mesopores and micropores of shales in the DD were quantitatively characterized by high-pressure mercury injection and nitrogen and CO_2 isothermal adsorption experiments. The results show that the SSA of macropores is 4.2 $\times$ 10^{-5}-1.14 m^2/g, with an average of 0.30 m^2/g; the SSA of mesopores is 0.25–17.95 m^2/g, with a mean of 4.70 m^2/g; and the SSA of micropores is 0.61–22.6 m^2/g, with an average of 6.60 m^2/g. Thus, mainly micropores and mesopores contribute to the SSA. Overall, the total SSA ranges from 1.09–33.68 m^2/g, with a mean of 11.59 m^2/g.

6. Discussion

6.1. Data error analyses

In this study, 59 shale samples were tested. As shown in Fig. 13, the TOC content and ($S_{11} + S_{21} + S_{22} + S_{23}$) are positively correlated, and the square of the fitting coefficient (R^2) is 0.8809, indicating that the results of the TOC content and pyrolysis tests and light hydrocarbon calibration were reliable. The evaluation parameter reliability of shale is affected by thermal maturity. Generally, the parameters are applicable when thermal maturity is low, while they cannot reflect the actual characteristics of shale (e.g., Rock-Eval pyrolysis, T_{max}) when maturity is high (Ro > 1.3%) (Peters 1986; Zhang et al. 2007). As described in Section 5.4, 96.8% of the shales in the DD are immature-mature (Fig. 15), indicating that it is reliable to use pyrolysis tests to analyze the geochemical characteristics of shale. However, when using the *T*max - HI plot to evaluate the organic matter type, it was found that there were two anomalous points in the lower right corner, whose *T*max values were abnormally high and whose organic matter type cannot be determined (Fig. 16). Further analyses showed that the organic matter richness of these two samples was very low, with TOC contents less than 0.23% (Fig. 13), indicating that these two samples were not source rocks and that the tested organic matter should be related to the migrated hydrocarbons. Therefore, the test data of these two samples are not considered in the subsequent discussion.

6.2. Factors controlling movable oil content

The factors controlling the movable oil content of shales are complex and are directly related to oil generation potential, oil storage capacity, and oil retention capacity (Wang et al. 2019a, b). The oil generation potential is related to the organic matter richness, type, and thermal

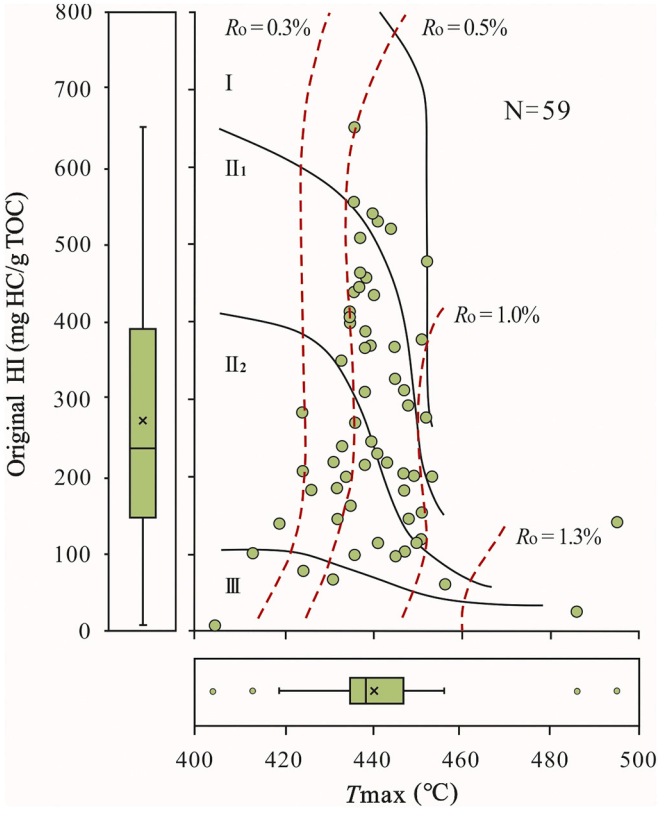

Fig. 16. Correlations between pyrolysis T_{max} and hydrogen index (HI) of the Paleogene shales in the Dongpu Depression. N indicates the number of samples.

maturity; the oil storage capacity is related to the pore volume, which is controlled by the organic matter richness and mineral composition; the oil retention capacity is related to adsorption capacity, which is controlled by mineral composition and SSA (Lu et al. 2016; Li et al., 2014, Li et al., 2020a; Liu et al. 2020).

6.2.1. *Organic matter richness*

Organic matter is the material basis for oil generation in shale. When the organic matter type and maturity are fixed, the higher the organic matter richness is, the stronger the oil generation capacity (Peters and Cassa 1994). As shown in Fig. 13, the movable oil content of shales in the DD is positively correlated with TOC, indicating that organic matter richness is a factor controlling movable oil content. However, the movable oil contents of some samples are low, even for a TOC content greater than 2%. This might be related to the different organic matter composition, mineral composition, and textures, which further resulted in different oil generation potential and oil storage space of shales with similar organic matter richness. This phenomenon can also be seen in previous studies on the strata in the DD (Li et al. 2020a), Lucaogou Fm. in the Jimusar Depression, Junggar Basin (Hu et al. 2018a), Hetaoyuan Fm. in the Biyang Sag, Nanxiang Basin (Feng et al. 2019), Qingshankou Fm. in the Songliao Basin (Lu et al. 2016), Xingouzui Fm. in the Jianghan Basin (Li et al. 2015a), and Shahejie Fm. in the Bonan Sag, Bohai Bay Basin (Lu et al. 2016).

From the envelope line, when TOC < 1%, the movable oil content increases rapidly with increasing TOC content; when 1% < TOC < 2%, the movable oil content increases continually with increasing TOC content but with a decreasing rate of increase; when TOC > 2%, the movable oil content maintains a high value with increasing TOC content (Fig. 13). This is consistent with the "trichotomy" relationship between the oil content and TOC content in the Lucaogou Fm. in the Jimusar Depression (Hu et al. 2018a), the Hetaoyuan Fm. in the Biyang Sag (Feng et al. 2019), the Qingshankou Fm. in the Songliao Basin (Lu et al. 2016),

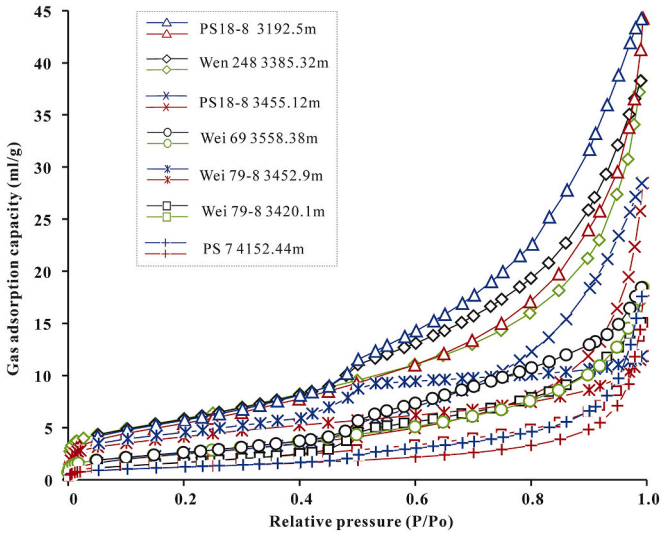

Fig. 18. Nitrogen and carbon dioxide adsorption-desorption isotherms of the Paleogene shales in the Dongpu Depression.

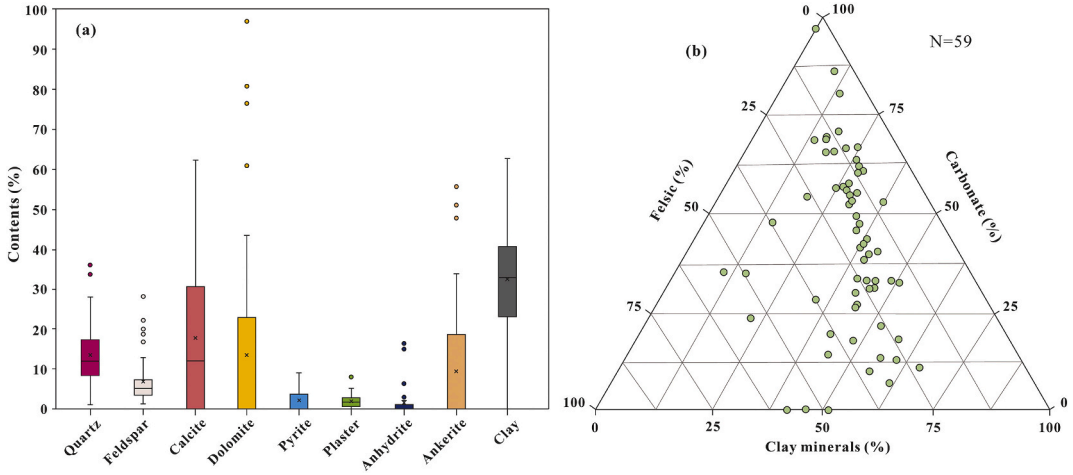

Fig. 17. Mineral composition of the Paleogene shales in the Dongpu Depression. (a) Box chart showing the mineral composition; (b) Ternary diagram showing the relative ratio of felsic, carbonate, and clay minerals.

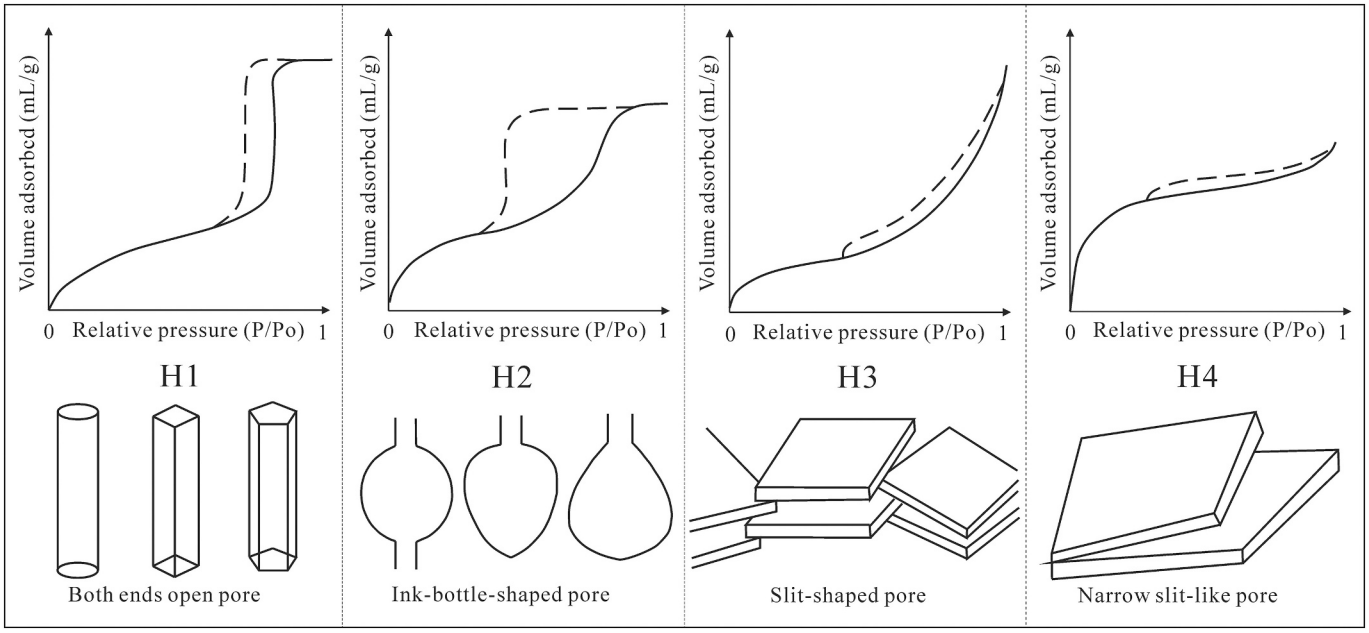

Fig. 19. Adsorption-desorption isotherm types with hysteresis loops and their corresponding pore shapes (modified from Sing et al. 1985).

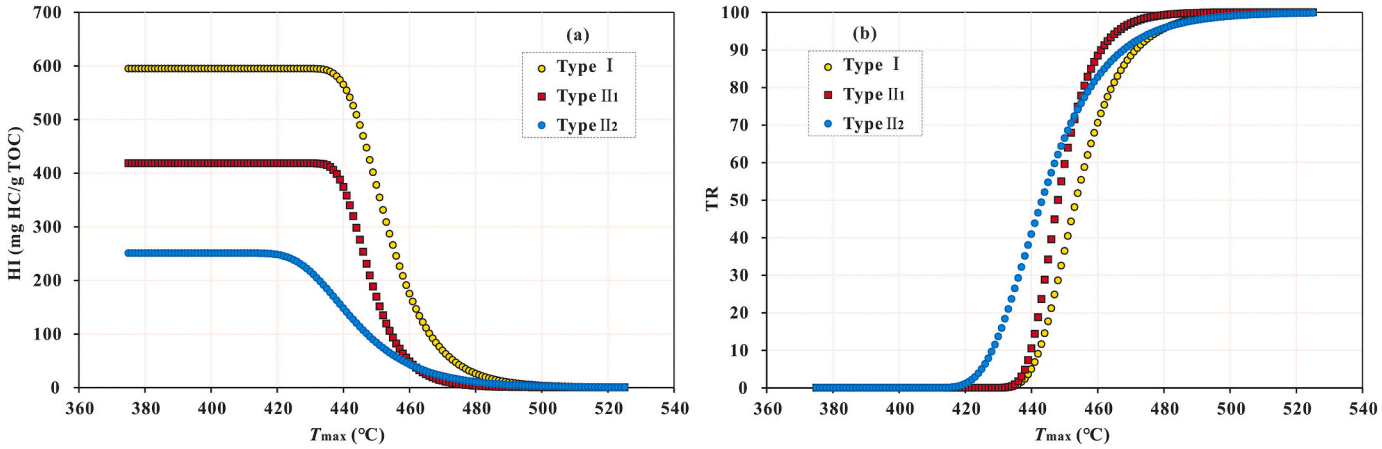

Fig. 20. Hydrocarbon generation potential (a) and TR (transformation ratio) (b) of different types of kerogen source rocks as data driven modelled from their Rock-Eval data.

the Xingouzui Fm. in the Jianghan Basin (Li et al. 2015a) and the Shahejie Fm. in the Bonan Sag (Lu et al. 2016). Only shales with abundant organic matter are favorable for the formation of shale oil plays with commercial value (Jarvie 2008, 2012; Wang et al. 2019a). When organic-rich shales start to generate oil, the oil first undergoes (mineral and kerogen) adsorption/swelling in place (O'Brien et al., 2002; Jarvie, 2012; Larter et al. 2012), but when the TOC content is low, the generated oil amount is small and is unable to reach the in-place adsorption/swelling capacity, so the oil is incapable of being expelled. With increasing TOC content, when the oil generated from shales meets the in-place adsorption/swelling limits, the oil is retained in pores and fractures in a free state (Pang et al., 1993a, b, 2005), and the movable oil content increases gradually. When the TOC content continues to increase, due to the limited pore and fracture spaces available for oil retention, the additional generated oil will migrate and be expelled. Therefore, the movable oil content will remain at an elevated value and no longer increase or increase slightly with increasing TOC content. Due to differences in the organic matter sources and mineral compositions of shales in different areas, the development and evolution of pores and fractures are different; hence, the boundaries of the "trichotomy" vary for different areas. For example, the critical TOC contents of the Lucaogou Fm. in the Jimusar Depression are 1.7% and 3.4% (Hu et al. 2018a); the critical TOC contents of the Shahejie Fm. in the Bonan Sag are 0.8% and 2.4% (Lu et al. 2016); and the critical TOC contents of the Xingouzui Fm. in the Jianghan Basin are 0.75% and 1.9% (Li et al. 2015a).

6.2.2. *Organic matter type*

The organic matter type of shale is related to its origin. Organic matter with different origins has different chemical compositions and structures and thus different oil generation capacities. For Type I kerogen, the organic matter mainly originates from algae, bacteria and some other lower aquatic organisms and has a strong oil generation capacity (Marchand et al. 1969). The organic matter of Type III kerogen mainly originates from terrigenous higher plants, and its oil generation capacity is limited (Combaz 1980). Therefore, in addition to organic

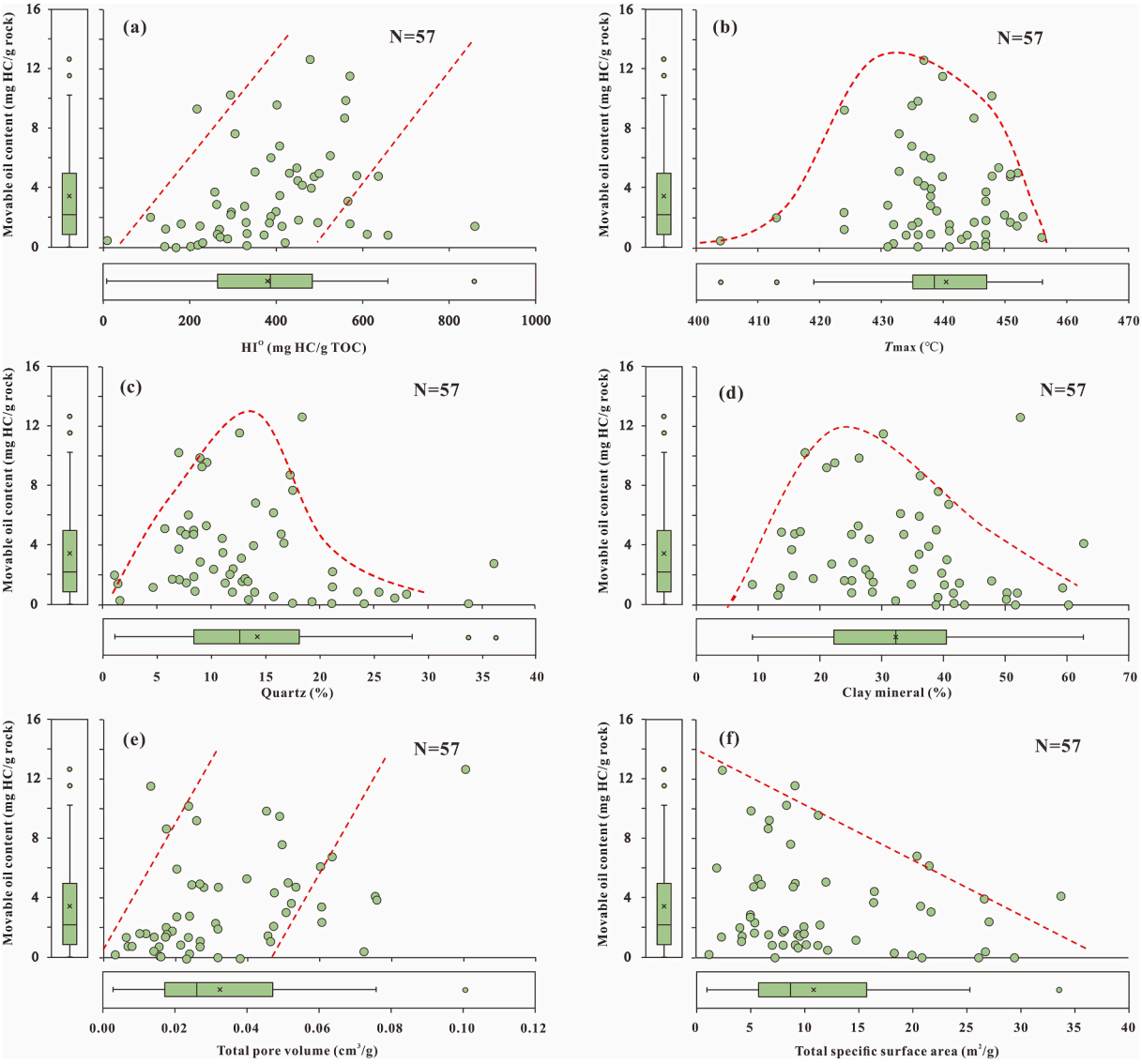

Fig. 21. Correlations among movable oil contents ($S_{11} + S_{21}$) and controlling factors of the Paleogene shales in the Dongpu Depression. N indicates the number of samples.

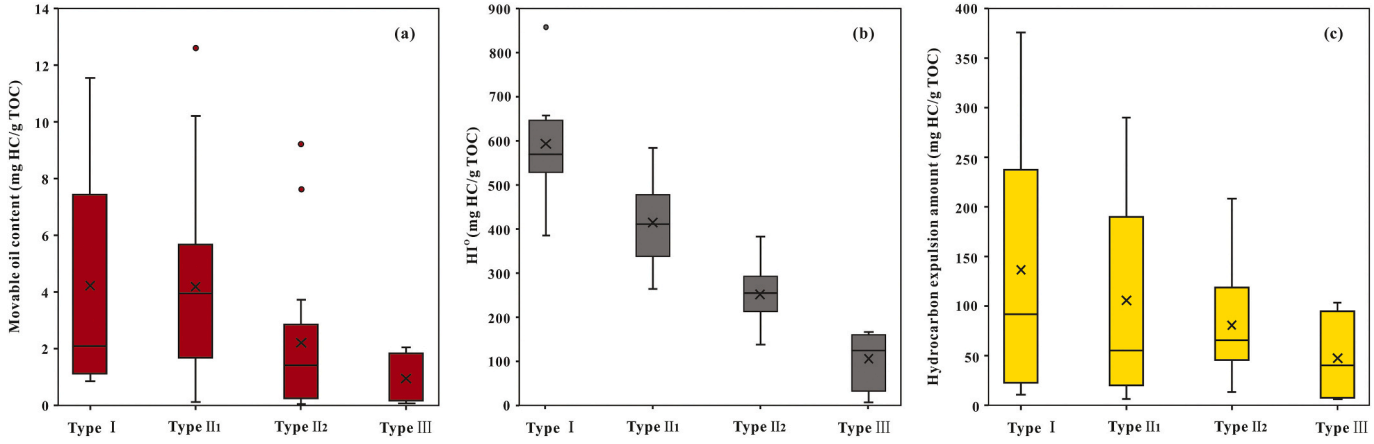

Fig. 22. Comparison of (a) movable oil contents ($S_{11} + S_{21}$), (b) original HI (HI^{o}), and (c) hydrocarbon expulsion amounts in Paleogene shales with different kerogen types of the DD.

matter richness, organic matter type is an important index for determining oil generation capacity. However, due to the common qualitative and semiquantitative classifications of organic matter types, such as classification schemes of Type I, Type II_1, Type II_2, and Type III, few studies have analyzed the influence of organic matter type on movable oil content (Li et al., 2014). The kerogen type index (KTI), which is calculated with the maceral composition and organic element data of the kerogen, is commonly used for characterizing organic matter type quantitatively, but the testing procedures are complex. Many researchers use the HI to identify organic matter type: the higher the HI, the closer to Type I the organic matter is, and thus the stronger the oil generation capacity will be. For example, HI > 600 mg HC/g TOC, 300–600 mg HC/g TOC, 200–300 mg HC/g TOC, and < 200 mg HC/g TOC, correspond to Type I kerogen, Type II_1 kerogen, Type II_2 kerogen, and Type III kerogen, respectively (Peters and Cassa 1994). Notably, most of the tested shale samples passed the HET, and the obtained pyrolysis data did not reflect the original characteristics of the shale. In other words, the HI doesn't represent the original oil generation capacity (HI^o). Therefore, it is necessary to restore HI^o to reflect the organic matter types more accurately. In this study, a data-driven model for studying kerogen kinetics was utilized to reconstruct HI^o (Fig. 20) (Chen and Jiang 2015). This model holds that petroleum generation kinetics of kerogen in a certain organic-rich shale can be characterized by its reaction path along thermal maturation (Chen and Jiang 2015), and hence the HI^o can be restored by the most commonly accessible Rock-Eval/TOC data. However, this model fails to consider certain maceral composition and organic matter type of kerogen and the geological conditions of the shales developed (Chen and Jiang 2015). Try to avoid this issue, this model was utilized after the organic matter types were classified. The specific formula is shown in Eqs. 6–7.

$$H_I = H_I^0\left\{1 - exp\left[-\left(\frac{T_{max}}{\beta}\right)^{\theta}\right]\right\} + c \tag{6}$$

$$T_R = \frac{1200}{H_I^0}\frac{\left(H_I^0 - H_I\right)}{(1200 - H_I)} \tag{7}$$

HI^o is the original HI, mg HC/g TOC; HI is the hydrogen index (S_2/TOC), mg/g; T_{max} is the maximum temperature of the pyrolysis peak, °C; T_R is the kerogen conversion rate corresponding to pyrolysis temperatures, %; β, θ and C are obtained by pyrolysis data simulation (Chen and Jiang 2015).

Analyses show that the movable oil content is positively correlated with HI^o (Fig. 21a), indicating that the stronger the initial oil generation potential is, the higher the movable oil content. However, an obvious anomaly occurred: four samples with HI^o values greater than 600 mg HC/g TOC, have low movable oil contents. The analyses performed suggest that these four samples are Type I kerogen (Fig. 21a), for which the low movable oil content may be related to the high oil expulsion efficiency (Fig. 22). Among these types of kerogen, Type I has the highest oil generation capacity, but it also has the highest oil expulsion efficiency. Generally, oil expulsion efficiency increases gradually as the kerogen type transitions from Type III to Type II_2, Type II_1 and Type I (Sandvik et al., 1992; Stainforth 2009; Zou et al. 2019). For Type I kerogen, the highest oil expulsion efficiency is related to strong oil generation capacity, under which conditions overpressure can easily form in the shale. Overpressure promotes fracture development, which in turn accelerates oil expulsion (Wang et al. 2015a, 2015c). In addition, organic acids form during or before oil generation and promote the formation of numerous secondary pores by the dissolution of minerals such as quartz and feldspar (Surdam et al. 1989; Yuan et al. 2019), which are important pore spaces for shale oil accumulation. Unlike Type II_2, Type II_1 and Type III kerogen, Type I kerogen is rich in hydrogen but poor in oxygen. Oxygen is an essential element for organic acid formation; thus, the secondary pores of Type I kerogen are less developed (Surdam et al. 1989), which is not conducive to shale oil enrichment. This phenomenon can also be seen in the Lucaogou Fm. shales in the Jimusar Depression (Hu et al. 2018a).

6.2.3. Thermal maturity

With a certain organic matter richness and type, the higher the thermal maturity, the more oil is generated; thus, thermal maturity may also be an index affecting the movable oil content of shales. The analyses show that the movable oil content of shale first increases and then decreases with increasing T_{max} (Fig. 21b). The movable oil content peaks at a T_{max} of 437 °C, indicating that the highest movable oil content occurs during early maturity. This should be related to both oil generation and expulsion and oil cracking. Specifically, the movable oil content increases gradually with oil generation during the early mature stage.

With increasing maturity, the shales start to expel oil only after the generated oil reaches the in-place adsorption, swelling, water dissolution and pore residue limits (Momper 1978; Pang et al., 1993a, b, 2005), so the movable oil content increases gradually before the HET. Oil expulsion occurs as long as the shales reach the HET, and the liquid oil may also start to crack (Li et al. 2015b), resulting in a decreasing movable oil content. Notably, this change is significantly different from that induced by the influence of thermal maturity on shale oil mobility. The higher the thermal maturity, the more light components there are, which results in a high gas-oil ratio and better oil mobility (Wang et al., 2018; Li et al. 2020a).

6.2.4. Quartz content

Movable oil content is related to the physical properties of the shale. The mineral composition and proportions influence the pore and fracture development of shale and, in turn, determine its physical properties (Curtis, 2002a, b; Kuila and Prasad 2013; Liu and Peng 2017). The primary pore space is the effective pore space for oil enrichment and is related to the quantity of terrigenous debris input, which can be characterized by quartz content (Chen et al. 2011; Dong et al., 2019). Analyses show that the movable oil content of the shales first increases and then decreases with increasing quartz content, peaking at a quartz content of 15% (Fig. 21c). This may be due to two reasons. First, primary pore development is related to terrigenous debris input quantity. The higher the quartz content, the larger the primary pores are (Dong et al., 2019; Feng et al. 2019). Second, the quartz content is intrinsically related to the TOC content (Rowe et al. 2008; Liu et al. 2019). Because the movable oil content is positively correlated with the TOC content, the quartz content has some correlation with movable oil content. Generally, increasing quartz content indicates an increasing amount of terrestrial debris input, which would provide large amounts of nutrients to the depositional water and is favorable for the existence of lower aquatic organisms, even prompting algae blooms (Bohacs et al. 2005; Wu et al. 2014). Therefore, the paleoproductivity would increase greatly, and the TOC content would also increase. The terrigenous debris input quantity continuously increases with the quartz content. While the space suitable for organism existence of depositional water is certain, when the paleo-productivity peaks, the terrigenous debris input quantity will dilute the sedimentary organic matter, decreasing the TOC content. Specifically, in shales of the DD, the TOC content decreases gradually with increasing quartz content when the quartz content surpasses 15%. Due to the strong positive correlation between TOC content and movable oil content, the correlation between quartz content and the movable oil content initially increases and then decreases.

6.2.5. Clay mineral content

The stronger the adsorption capacity is, the lower the movable oil content (Li et al. 2018a). The adsorption capacity of shale is directly related to the clay mineral content (Feng et al. 2019). The analyses show that the movable oil content of the shales increase initially and then decrease with increasing clay mineral content, peaking at a clay mineral content of 25% (Fig. 21d). This is inconsistent with previous studies that concluded that the movable oil content decreases with increasing clay

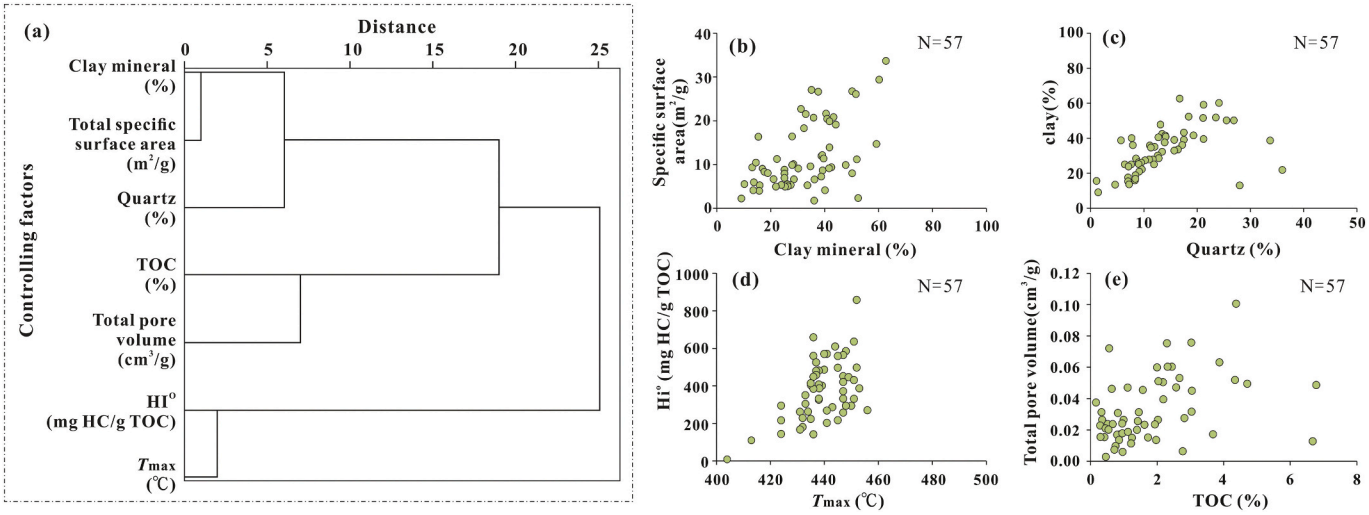

Fig. 23. Analyses of factors controlling movable oil contents ($S_{11} + S_{21}$). (a) Systematic cluster analysis by the IBM SPSS Statistics 25 software; (b) Correlation between clay minerals and SSA; (c) Correlation between quartz and clay minerals; (d) Correlation between T_{max} and original HI (HI^{o}); (e) Correlation between TOC and total pore volumes.

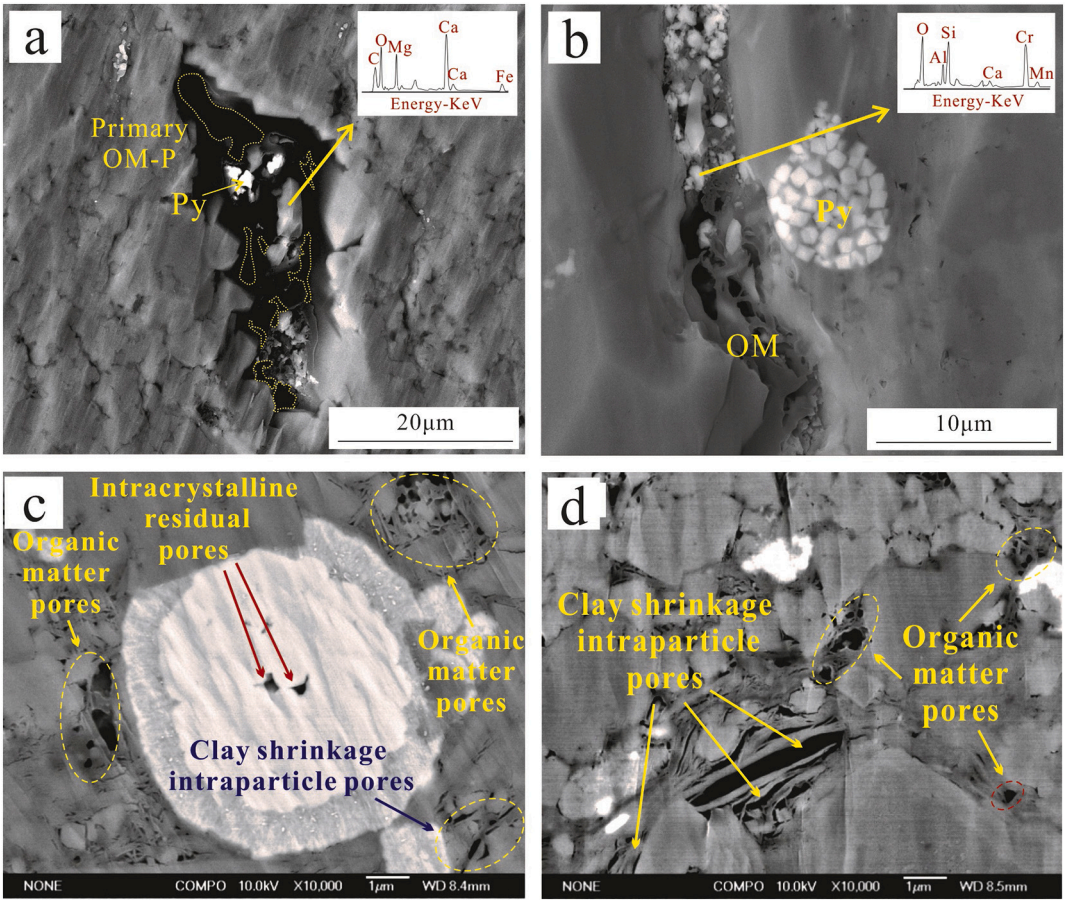

Fig. 24. Organic matter pores of the Paleogene shales of the DD. (a) Well Wei 42, 3461.65 m; (b) Well PS 13, 5011.01 m; (c) Well PS18–1, 3267 m; (d) Well PS18–8, 3167.2 m. ((a)-(b) were cited from Shao et al. 2018).

mineral content (Feng et al. 2019). This difference may have two explanations. First, the movable oil content is correlated with the adsorption capacity of shales, which in turn is related to the clay mineral content. The higher the clay mineral content, the stronger the adsorption capacity is, and thus the lower the movable oil content. Second, the clay mineral content is intrinsically related to TOC content. Because movable oil content is positively correlated with TOC content, the clay mineral content has some correlation with movable oil content. Generally, the clay mineral content is a practical index for indicating water turbulence during deposition (Bohacs et al. 2005; Liu et al. 2007); the higher the clay mineral content is, the lower the turbulence. Therefore, the higher the clay mineral content, the better the preservation condition for

Table 3
Movable oil content prediction of the randomly selected ten shale samples.

Smaple NO.	Depth (m)	TOC (%)	Calibrated ($S11+S21$) (mg/g)	Total pore volume (cm^3/g)	Totail SSA (m^2/g)	Predicted ($S11+S21$) (mg/g)
13	3184.9	0.96	1.43	0.006	2.247	2.37
21	3677.81	2.19	5.34	0.040	5.612	5.19
22	3188.8	2.32	2.44	0.060	27.057	3.53
23	3167.22	6.78	9.58	0.049	11.288	11.08
24	3155.12	2.58	4.46	0.047	16.430	4.73
26	3282.66	2.45	3.47	0.060	20.728	4.52
29	3685.7	1.12	2.20	0.047	11.366	3.12
41	3279.2	4.71	7.65	0.049	8.680	9.07
43	3159.12	0.46	0.26	0.003	1.092	1.61
55	3558.38	0.64	1.20	0.046	14.723	1.94

organic matter accumulation is, and thus the higher the TOC content is. However, when the clay mineral content exceeds a critical value, the depositional water is too calm and lacks nutrient input, which indicates that the depositional setting is not favorable for supporting aquatic organisms, resulting in a low paleoproductivity and TOC content (Bohacs et al. 2005; Wu et al. 2014; Chen et al. 2011). Because the movable oil content is positively correlated with TOC content, the relationship between the clay mineral content and movable oil content initially increases and then decreases. Specifically, in shales of the DD, the TOC content decreases gradually with increasing clay mineral content when the clay mineral content is greater than 25%.

Under combined control of the above two explanations, when clay mineral content is less than 25%, increasing clay mineral content both promotes increasing TOC content and adsorption capacity of shales, but impacts of increasing TOC content on movable oil content are significantly greater than that of the increasing adsorption capacity, thus the movable oil content increases. When clay mineral content surpasses 25%, increasing clay mineral contents also promote increasing TOC content and adsorption capacity simultaneously, but impacts of increasing TOC content on movable oil content are lower than that of the increasing adsorption capacity, thus the movable oil content decreases gradually (Fig. 21d).

6.2.6. Pore volume

Abundant micro−/nanoscale pores develop in shales and are key storage spaces for oil. As shown in the microscopic images of oil-generating biota and FE-SEM (field emission scanning electron microscopy), large amounts of bitumen were distributed in the intergranular pores of the calcium-rich carbonate laminas in the studied shale, with weak orange yellow fluorescence (Fig. 14). Therefore, the pore volume

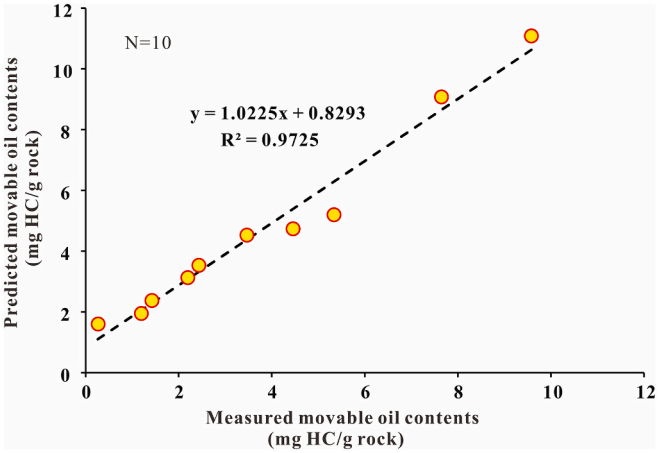

Fig. 26. Validation of the established model by comparing the measured and predicted movable oil contents. N indicates the number of samples.

directly affects the movable oil content (Loucks et al. 2012; Zou et al. 2019; Zhu et al., 2019b). The analyses show that the movable oil content of the shales increase with increasing pore volume (Fig. 21e). This finding is similar to those from other lacustrine shale oil plays (Li et al., 2014; Feng et al. 2019). Before reaching the HET, the oil generated from the shales is preferentially retained in pores after satisfying the in-place adsorption/swelling limits. When these pores became saturated, the additional oil generated was expelled with an episodic expulsion pattern (Roberts and Nunn 1995; Ma et al. 2016). The larger the pore volumes, the greater the spaces for oil retention are, and thus the greater the movable oil content is.

6.2.7. SSA

Clay minerals and pores are key contributors to the SSA of shale (Kuila et al. 2014; Liu and Peng, 2017). Generally, the greater the SSA is, the stronger the adsorption capacity (Li et al. 2018a). The analyses show that the movable oil content of the shales decreases with increasing total SSA (Fig. 21f), indicating that when pore volumes remain the same, the larger the SSA is, the lower the movable oil content. This finding is consistent with the results of prior studies (Feng et al. 2019).

6.3. Movable oil content estimation model

Based on the above analyses, the movable oil content of the shales has certain correlations with organic matter richness, type, and thermal maturity, quartz content, clay mineral content, pore volume, and total

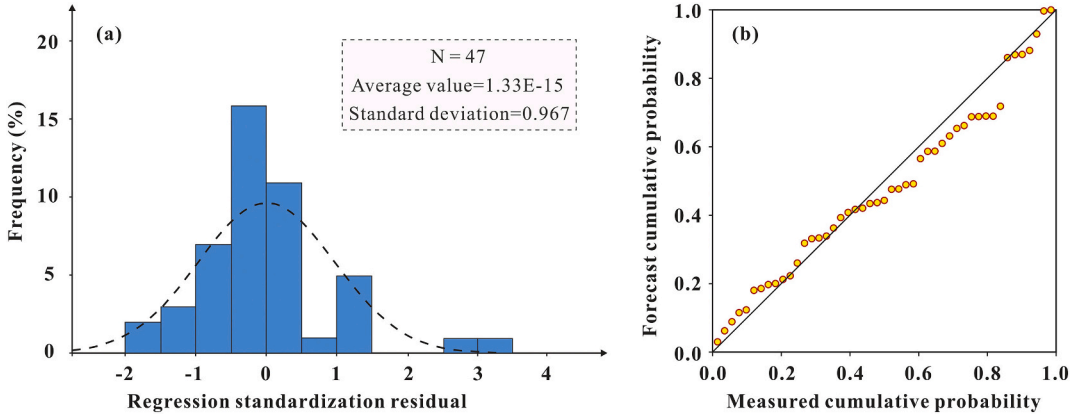

Fig. 25. Accuracy validation of the numerical simulation results by regression standardized residual and cumulative probability with the IBM SPSS Statistics 25 software.

SSA. However, there may also be some internal relationships among the above seven factors, such as the internal relationship that exists among the TOC, quartz, and clay mineral contents and also the clay minerals and SSA (Kuila et al. 2014; Liu and Peng, 2017). Given this, IBM's SPSS Statistics 25 software was utilized in this study to a conduct systematic cluster analysis on the above seven factors to determine the unique factors affecting movable oil content (for example, the intergroup connection and Pearson correlation tests were utilized). The systematic cluster analysis shows that the clay mineral content is positively correlated with total SSA (Fig. 23a), indicating that the key contributor to the SSA of the shales is the clay mineral content (Fig. 23b). Meanwhile, quartz content shows a weak correlation with the clay mineral content and total SSA, which may be related to the inherent correlation between the quartz and clay mineral contents in lacustrine deposits (Fig. 23c). HI^o is correlated with T_{max}, probably because T_{max} is included in the data-driven model for reconstructing kerogen kinetics (Fig. 23d). There is a high correlation between the TOC content and total pore volume, indicating that many organic matter pores developed in the studied shales, and are key contributors to the total pore volume (Fig. 24).

IBM SPSS Statistics 25 was utilized to conduct a multiple regression analysis of factors controlling the movable oil content and ultimately establish a movable oil content evaluation model. The results show that the standardized coefficients of the movable oil content of the shales with the above seven parameters are significantly different. Among them, the standardized coefficients of the TOC content, total pore volume and total SSA are much greater than those of HI^o, T_{max}, and the quartz and clay mineral contents, indicating that TOC content, pore volume and SSA are the key factors controlling movable oil content. Therefore, based on the system cluster analysis results and on a guaranteed basis of model accuracy, TOC content, pore volume and SSA were used in the simulation to establish the movable oil content evaluation model. Notably, to assess the accuracy of the model, 47 tested shale sample data points were randomly selected in this study for multiple regression simulation (Table 3), and the remaining 10 data points were utilized to validate the accuracy of the model (Table 3). The established model is shown in Eq. 8.

$$Y = 1.531 \times X_1 + 40.764 \times X_2 - 0.126 \times X_3 + 0.932 \quad (8)$$

X_1 is TOC, %; X_2 is total pore volume, cm^3/g; X_3 is total SSA, m^2/g.

To some extent, this evaluation model removes the limitations that most of the existing methods display. This approach makes full use of the data obtained in previous studies, overcomes the problem of a lack of shale cores, and provides ways for reducing testing costs. However, the accuracy and reliability of the predicted movable oil content are related to the reliability of existing test data. Meanwhile, there are three aspects to be noted: There is not necessarily a correlation between movable oil content and shale oil mobility. The movable oil content could be high with poor oil mobility. In addition to the movable oil content, the shale oil mobility is also controlled by the oil composition, oil maturity, fracture development density, and formation pressure. ② The shale core samples studied in this work mainly come from the Es Fm. of the DD, which developed in a brackish-saline lacustrine environment, and the organic matter types are mainly Type II and Type I, with Type II_1 dominating. Therefore, the established evaluation model might not be applicable for shales deposited in fresh or ultra-saline lacustrine environments, marine shales, or shales with Type III and Type II_2 kerogen. It is suggested that studies on the factors controlling the movable oil content should be conducted on fresh lacustrine shale, ultra-saline lacustrine shale, marine shales, and shales with Type III and Type II_2 kerogen to establish a corresponding evaluation model. ③ If a more accurate evaluation model of movable oil content is required, due to the strong heterogeneity of lacustrine shales, it is necessary to further classify the shales into different lithofacies by using the TOC content, mineral composition, and rock textures, then analyze key factors controlling the movable oil content, and finally establish a movable oil content evaluation model for shales with different lithofacies.

6.4. Accuracy validation

Numerical simulation results show that R^2 of the regression evaluation model reaches 0.791 and that the regression standardized residual conforms to a normal distribution (Fig. 25). Therefore, the evaluation model established by multiple regression is reliable. In addition, based on the TOC content, pore volume and SSA data of the remaining 10 shale samples, the movable oil content was predicted by the evaluation model. The results show that the predicted movable oil content was consistent with the tested movable oil content with a linear fitting equation coefficient of 1.0253 and R^2 of 0.9725 (Fig. 26), which further validated the accuracy of the model.

7. Summary and conclusions

This paper provides an extensive review of the theories, techniques, and methods of movable oil content evaluation and their merits and demerits for lacustrine shales. Taking typical lacustrine shales of the Paleogene Shahejie Fm. (50.5–33 Ma) of the DD and Bohai Bay Basin as an example, a novel and practical quantitative model for movable oil content evaluation was established. The main conclusions are as follows.

(1) A brief review of the OSI, GEM, HETM, POSM, MREPM, MSEM, FHDM, SM, NMR, and MDS methods for movable oil content evaluation and their limitations for lacustrine organic-rich shales was provided. The MREPM combined with light hydrocarbon calibration is the most mature and practical method of the movable oil content evaluation for lacustrine shales.

(2) The movable oil content of the Es Fm. shales in the DD are high; 71.2% of the studied samples resulted in oil crossover effects, reflecting a high organic matter richness and oil-prone organic matter types within the oil window. The mineral composition is complex, for which carbonate is found in the highest proportion, followed by clay minerals, and the felsic mineral content is the lowest. The shale pores are mainly macropores and mesopores, and the total pore volume ranges from 2.8–100.6 × 10−3 cm3/g, with an average of 32.5 × 10−3 cm3/g. The SSA is mainly controlled by the micropores and mesopores, and the total SSA ranges from 1.09–33.68 m2/g, with a mean of 11.59 m2/g.

(3) The TOC content, pore volume and SSA are the key factors controlling the movable oil content of these shales, and the evaluation model was simulated by IBM SPSS Statistics 25 and validated with test data.

(4) In the future, due to the strong heterogeneity of lacustrine shales, it is necessary to establish movable oil content evaluation models for shales with different lithofacies for a more accurate evaluation.

Declaration of Competing Interest

We declare that we do not have any commercial or associative interest that represents a conflict of interest in connection with the work submitted.

Acknowledgments

This study was financially supported by the China Postdoctoral Science Foundation (2019M660054), Science Foundation of China University of Petroleum (Beijing) (2462019BJRC005), National Natural Science Foundation of China (41872148, 41872128), 2017 AAPG Foundation Grants-in-Aid Program (15388), Strategic Cooperation Technology Projects of CNPC and CUPB (ZLZX2020-01-05), China Major Science 973 Project (2011CB2011-02 and 2014CB239101), and the Science Projects of the Sinopec Zhongyuan Oilfield Company (P15022).

References

Ambrose, R.J., Hartman, R.C., Diaz-Campos, M., Akkutiu, I.Y., Sondergeld, C.H., 2012. Shale gas-in-place calculations part I: new pore-scale considerations. SPE J. 17 (1), 219–229. https://doi.org/10.2118/131772-PA.

Behar, F., Beaumont, V., De, H.L., Penteado, B., 2001. Rock-Eval 6 technology: Performances and developments. Oil Gas Sci. Technol. 56 (2), 111–134.

Behar, F., Beaumont, V., Penteado, H.L.D.B., 2002. Rock-Eval 6 technology: performances and development. Oil Gas Sci. Technol. 56 (2), 111–134. https://doi.org/10.2516/ogst:2001013.

Birdwell, J.E., Washburn, K.E., 2015. Multivariate analysis relating oil shale geochemical properties to NMR relaxometry. Energy Fuel 29, 2234–2243.

Bohacs, K.M., Grabowski, G.J., Carroll, A.R., Mankiewicz, P.J., Miskell, K.J., Schwalbach, J.R., 2005. Production, Destruction, and Dilution-The Many Paths to Source-Rock Development. The Deposition of Organic-Carbon-Rich Sediments: Models, Mechanisms, and Consequences. SEPM Society for Sedimentary Geology, pp. 61–101. https://doi.org/10.2110/pec.05.82.0061.

Cai, J.G., Bao, Y.J., Yang, S.Y., Wang, X.X., Fan, D.D., Xu, J.L., Wang, A.P., 2007. Research on preservation and enrichment mechanisms of organic matter in muddy sediment and mudstone. Sci. China Ser. D Earth Sci. 50 (5), 765–775.

Cao, H.R., Zou, Y.R., Lei, Y., Xi, D.P., Wan, X.Q., Peng, P.G., 2017. Shale Oil Assessment for the Songliao Basin, Northeastern China, using Oil Generation - Sorption Method. Energy Fuel 31 (5), 4826–4842. https://doi.org/10.1021/acs.energyfuels.7b00098.

Chen, Z.H., Jiang, C.Q., 2015. A data driven model for studying kerogen kinetics with application examples from Canadian sedimentary basins. Mar. Pet. Geol. 67, 795–803. https://doi.org/10.1016/j.marpetgeo.2015.07.004.

Chen, S.B., Zhu, Y.M., Wang, H.Y., Liu, H.L., Wei, W., Fang, J.H., 2011. Shale gas reservoir characterisation: a typical case in the southern Sichuan Basin of China. Energy 36 (11), 6609–6616. https://doi.org/10.1016/j.energy.2011.09.001.

Chen, L., Jiang, Z.X., Liu, K.Y., Tan, J.Q., Gao, F.L., Wang, P.F., 2017. Pore structure characterization for organic-rich lower Silurian shale in the Upper Yangtze Platform, South China: a possible mechanism for pore development. J. Nat. Gas Sci. Eng. 46, 1–15.

Clementz, F.S., 1979. Effect of oil and bitumen saturation on source rock pyrolysis. AAPG Bull. 63, 2227–2232.

Combaz, A., 1980. Les kérogènes vus au microscope. In: Durand, B. (Ed.), Kerogen. Technip, Paris, pp. 55–111.

Curtis, J.B., 2002a. Fractured shale - gas systems. AAPG Bull. 86 (11), 1921–1938. https://doi.org/10.1306/61EEDDBE-173E-11D7-8645000102C1865D.

Curtis, J.B., 2002b. Fractured shale-gas system. AAPG Bull. 86, 1921–1938.

Dang, S.T., Sondergeld, C.H., Rai, C.S., 2018. Interpretation of nuclear-magnetic-resonance response to hydrocarbons: application to miscible enhanced-oil-recovery experiments in shales. SPE Reserv. Eval. Eng. 191144.

Daughney, C.J., 2000. Sorption of crude oil from a non-aqueous phase onto silica: the influence of aqueous pH and wetting sequence. Org. Geochem. 31, 147–158.

Dong, T., Harris, N.B., Mcmillan, J.M., Twemlow, C.E., Nassichuk, B.R., Bish, D.L., 2019. A model for porosity evolution in shale reservoirs: an example from the Upper Devonian Duvernay Formation, Western Canada Sedimentary Basin. AAPG Bull. 103 (5), 1017–1044. https://doi.org/10.1306/10261817272.

EIA, 2013. Technically Recoverable Shale Oil and Shale Gas Resources: An Assessment of 137 Shale Formation in 41Countries Outside the United States, Washington.

EIA, 2019a. International Energy Outlook. https://www.eia.gov/outlooks/ieo.

EIA, 2019b. Weekly Petroleum Status Report. https://www.eia.gov/petroleum/supply/weekly.

Espitalié, J., 1982. Methode pratique de caracterisation des roches mere et des zones de formation du petrole. Petrol. Techn. 283, 99.

Espitalié, J., Madec, M., Tissot, B.P., Mening, J.J., Leplate, P., 1977. Source rock characterization method for petroleum exploration. In: Proceedings of 9th Annual Offshore Technology Conference, Houston, Texas, May 2–5, pp. 439–448.

Exxon, M., 2018. Outlook for Energy: A View to 2040. http://corporate.exxonmobil.com/en/energy/energyoutlook/a-view-to-2040.

Feng, G.Q., Li, J.J., Liu, J.W., Zhang, X.W., Yu, Z.Y., Tan, J.J., 2019. Discussion on the enrichment and mobility of continental shale oil in Biyang Depression. Oil Gas Geol. 40 (06), 1236–1246. https://doi.org/10.11743/ogg20190608.

Fleury, M., Romero-Sarmiento, M., 2016. Characterization of shales using T1–T2 NMR maps. J. Petrol. Sci. Eng. 137, 55–62.

Guan, P., Xu, Y.C., Liu, W.H., 1998. Quantitative estimates of different existing state of organic matter in source rocks. Chin. Sci. Bull. 43 (14), 1556–1559.

Harrison, A., Cracknell, R.F., Krueger-Venus, J., Sarkisov, L., 2014. Branched versus linear alkane adsorption in carbonaceous slit pores. Adsorption 20, 427–437.

Hopkins, A.S., 2017. The next energy economy. Science 356 (6339), 709. https://doi.org/10.1126/science.aam8696.

Hu, T., Pang, X.Q., Yu, S., Wang, X.L., Pang, H., 2016. Hydrocarbon generation and expulsion characteristics of lower Permian P1f source rocks in the Fengcheng area, northwest margin, Junggar Basin, NW China: implications for tight oil accumulation potential assessment. Geol. J. 51, 800–900.

Hu, T., Pang, X.Q., Jiang, S., Wang, Q.F., Zheng, X.W., Ding, X.G., Zhao, Y., Zhu, C.X., Li, H., 2018a. Oil content evaluation of lacustrine organic-rich shale with strong heterogeneity: a case study of the Middle Permian Lucaogou Formation in Jimusaer Sag, Junggar Basin, NW China. Fuel 221, 196–205. https://doi.org/10.1016/j.fuel.2018.02.082.

Hu, T., Pang, X.Q., Jiang, S., Wang, Q.F., Xu, T.W., Lu, K., Huang, C., Chen, Y.Y., Zheng, X.W., 2018b. Impact of Paleosalinity, Dilution, Redox, and Paleoproductivity on Organic Matter Enrichment in a Saline Lacustrine Rift Basin: a Case Study of Paleogene Organic-Rich Shale in Dongpu Depression, Bohai Bay Basin, Eastern China. Energy Fuel 32, 5045–5061. https://doi.org/10.1021/acs.energyfuels.8b00643.

Hughes, J.D., 2013. Energy: a reality check on the shale revolution. Nature 494 (7437), 307. https://doi.org/10.1038/494307a.

Hunt, J.M., 1967. The origin of petroleum in carbonate rocks. In: Chilingar, G.V., Bissell, H.J., Fairbridge, R.W. (Eds.), Carbonate Rocks. Elsevier, New York, pp. 225–251.

Jarvie, D.M., 2008. Unconventional Shale Resource Plays: Shale-Gas and Shale-Oil Opportunities. Texas Chtistian Unversity, Wordwide Geochemistry.

Jarvie, D.M., 2012. Shale resource systems for oil and gas: part 2: Shale-oil resource systems. Shale reservoirs-giant resources for the 21st century. AAPG Mem. 97, 89–119.

Jarvie, D.M., 2014. Components and Processes Affecting Producibility and Commerciality of Shale Resource Systems. Geologica Acta 12 (4), 307–325. https://doi.org/10.1344/GeologicaActa2014.12.4.3.

Jarvie, D., Baker, D., 1984. Application of the Rock-Eval III oil show analyzer to the study of gaseous hydrocarbons in an Oklahoma gas well. In: The 187th American Chemical Society National Meeting. Geochemistry Division.

Jarvie, D.M., Senftle, J.T., Hughes, W., 1995. Examples and new applications in applying organic geochemistry for detection and qualitative assessment of overlooked petroleum reservoirs. In: Grimalt, J.O., Dorronsoro, C. (Eds.), Organic Geochemistry: Developments and Applications to Energy, Climate, Environment, and Human History: 17th International Meeting on Organic Geochemistry, pp. 380–382.

Jiang, Q.G., Li, M.W., Qian, M.H., Li, Z.M., Li, Z., Huang, Z.K., Zhang, C.M., Ma, Y.Y., 2016. Quantitative characterization of shale oil in different occurrence states and its application. Pet. Geol. Exp. 38 (06), 842–849. https://doi.org/10.11781/sysydz201606842.

Jin, Q., 2001. Importance and research about effective hydrocarbon source rocks (in Chinese with English abstract). Petrol. Geol. Recov. Effic. 8, 1–4.

Jin, Z.J., Bai, Z.R., Gao, B., Li, M.W., 2019. Has China Ushered in the Shale Oil and Gas Revolution? Oil Gas Geol. 40 (3), 451–458. https://doi.org/10.11743/ogg20190301.

Jorgensen, W.L., Madura, J.D., Swenson, C.J., 1984. Optimized intermolecular potential functions for liquid hydrocarbons. J. Am. Chem. Soc. 106 (22), 6638–6646.

Kamp, P.C., 2008. Smectite-illite-muscovite transformations, quartz dissolution, and silica release in shales. Clay Clay Miner. 56 (1), 66–81.

Karimi, S., Saidian, M., Prasad, M., Kazemi, H., 2015. Reservoir rock characterization using centrifuge and nuclear magnetic resonance: a laboratory study of middle bakken cores. In: SPE Annual Technical Conference and Exhibition. Society of Petroleum Engineers.

Katz, B.J., 1990. Controls on distribution of lacustrine source rocks through time and space. In: Katz, B.J. (Ed.), Lacustrine Basin Exploration: Case Studies and Modern Analogs, Am. Assoc. Pet. Geol. Mem, vol. 50, pp. 61–76.

Katz, B.J., 1995. Factors controlling the development of lacustrine petroleum source rocks-an Update. AAPG Studies in Geology, no. 40. In: Huc, A.Y. (Ed.), Paleogeography, Paleoclimate, and Source Rocks. AAPG, Tulsa, OK, pp. 61–79.

Katz, B.J., Lin, F., 2014. Lacustrine basin unconventional resource plays: Key differences. Mar. Pet. Geol. 56, 255–265. https://doi.org/10.1016/j.marpetgeo.2014.02.013.

Katz, B.J., Lin, F., 2020. Consideration of the limitations of thermal maturity with respect to vitrinite reflectance, T_{max} and other proxies. In: AAPG Bulletin (Ahead of Print Abstract). https://doi.org/10.1306/09242019261.

Kausik, R., Fellah, K., Feng, L., Simpson, G., 2017. High-and low-field NMR relaxometry and diffusometry of the bakken petroleum system. Petrophysics 58, 341–351.

Kieffer, B., Jove, C.F., Oelkers, E.H., Schott, J., 1999. An experimental study of the reactive surface area of the Fontainebleau sandstone as a function of porosity, permeability, and fluid flow rate. Geochim. Cosmochim. Ac. 63, 3525–3534.

Kirschbaum, M.A., Mercier, T.J., 2013. Controls on the deposition and preservation of the cretaceous Mowry Shale and frontier formation and equivalents, Rocky Mountain region, Colorado, Utah, and Wyoming. AAPG Bull. 97, 899–992.

Kuhn, P.P., Di, P.R., Hill, R., Lawrence, J.R., Horsfield, B., 2012. Three-dimensional modeling study of the low-permeability petroleum system of the Bakken Formation. AAPG Bull. 96 (10), 1867–1897. https://doi.org/10.1306/03261211063.

Kuila, U., Prasad, M., 2013. Specific surface area and pore-size distribution in clays and shales. Geophys. Prospect. 6, 341–361.

Kuila, U., McCarty, D.K., Derkowski, A., Fischer, T.B., Topor, T., Prasad, M., 2014. Nano-scale texture and porosity of organic matter and clay minerals in organicrich mudrocks. Fuel 135, 359–373. https://doi.org/10.1016/j.fuel.2014.06.036.

Lafargue, E., Marquis, F., Pillot, D., 1998. Rock-Eval 6 Applications in hydrocarbon exploration , production. and soil contamination studies. Oil Gas Sci. Technol. 53 (4), 421–437.

Larsen, J.W., Li, S., 1997. An initial comparison of the interactions of Type I and III kerogens with organic liquids. Org. Geochem. 26 (5-6), 305–309. https://doi.org/10.1016/S0146-6380(97)00016-8.

Larter, S.R., Huang, H.P., Snowdon, L., Bennett, B., 2012. What we do not know about self-sourced oil reservoirs: challenges and potential solutions. In: SPE 162777, pp. 1–4. https://doi.org/10.2118/162777-MS.

Law, B.E., Dickinson, W.W., 1985. Conceptual model for origin of abnormally pressured gas accumulations in low-permeability reservoirs. AAPG Bull. 69 (8), 1295–1304.

Li, J.J., Shi, Y.L., Zhang, X.W., Chen, X., Yan, Y.X., Zhu, J.X., Lu, S.F., Wang, M., 2014. Control factors of enrichment and producibility of shale oil: A case study of Biyang Depression. Earth Sci. 39 (7), 848–857. https://doi.org/10.3799/dqkx.2014.079.

Li, W.H., Lu, S.F., Xue, H.T., Zhang, P.F., Hu, Y., 2015a. Oil content in argillaceous dolomite from the Jianghan Basin, China: Application of new grading evaluation criteria to study shale oil potential. Fuel 143, 424–429. https://doi.org/10.1016/j.fuel.2014.11.080.

Li, J.J., Wang, W.M., Cao, Q., Shi, Y.L., Yan, X.T., Tian, S.S., 2015b. Impact of hydrocarbon expulsion efficiency of continental shale upon shale oil accumulations in eastern China. Mar. Pet. Geol. 59, 467–479. https://doi.org/10.1016/j.marpetgeo.2014.10.002.

Li, Z., Zou, Y.R., Xu, X.Y., Sun, J.N., Li, M.W., Peng, P.A., 2016a. Adsorption of mudstone source rock for shale oil – experiments, model and a case study. Org. Geochem. 92, 55–62. https://doi.org/10.1016/j.orggeochem.2015.12.009.

Li, S.F., Hu, S.Z., Xie, X.N., Lv, Q., Huang, X., Ye, J.R., 2016b. Assessment of shale oil potential using a new free hydrocarbon index. Int. J. Coal Geol. 156, 74–85. https://doi.org/10.1016/j.coal.2016.02.005.

Li, Z.M., Zheng, L.J., Jiang, Q.G., Ma, Z.L., Tao, G.L., Xu, E.S., Qian, M.H., Liu, P., Cao, T. T., 2018a. Simulation of hydrocarbon generation and expulsion for lacustrine organic-rich argillaceous dolomite and its implications for shale oil exploration. Earth Sci. 43 (02), 566–576. https://doi.org/10.3799/dqkx.2018.025.

Li, J.B., Huang, W.B., Lu, S.F., Wang, M., Chen, G.H., Tian, W.C., Guo, Z.Q., 2018b. Nuclear magnetic resonance T1-T2 map division method for hydrogen-bearing components in continental shale. Energy Fuel 32 (9), 9043–9054. https://doi.org/10.1021/acs.energyfuels.8b01541.

Li, W., Pang, X.Q., Snape, C., Zhang, B., 2019a. Molecular simulation study on methane adsorption capacity and mechanism in clay minerals: effect of clay type, pressure, and water saturation in shales. Energy Fuel 33 (2), 765–778.

Li, J., Wu, K.L., Chen, Z.X., Wang, W.Y., Yang, B., Wang, K., Luo, J., Yu, R.J., 2019b. Effects of energetic heterogeneity on gas adsorption and gas storage in geologic shale systems. Appl. Energy 251, 113368. https://doi.org/10.1016/j.apenergy.2019.113368.

Li, H., Li, J.J., Wang, B.H., Lu, K., Zhou, Y., Wang, M., Zhao, L.J., Song, Z.C., 2020a. Controlling factors of continental shale oil mobility and resource potential in Dongpu Sag, Bohai Bay Basin. Pet. Geol. Exp. 42 (04), 632–638. DOI: 11781/sysydz202004632.

Li, W.W., Cao, J., Shi, C.H., Xu, T.W., Zhang, H.A., Zhang, Y.X., 2020b. Shale oil in saline lacustrine systems: a perspective of complex lithologies of fine-grained rocks. Mar. Pet. Geol. 116, 104351. https://doi.org/10.1016/j.marpetgeo.2020.104351.

Li, J.B., Jiang, C.Q., Wang, M., Lu, S.F., Chen, Z.H., Chen, G.H., Li, J.J., Li, Z., Lu, S.D., 2020c. Adsorbed and free hydrocarbons in unconventional shale reservoir: a new insight from NMR T1-T2 maps. Mar. Pet. Geol. 116, 104311. https://doi.org/10.1016/j.marpetgeo.2020.104311.

Liu, Y., Peng, P.A., 2017. Research on the influences of different mineral compositions on the development of nanopores in shales. J. China Coal Soc. 42 (03), 702–711. https://doi.org/10.13225/j.cnki.jccs.2016.0580.

Liu, Z.F., Colin, C., Huang, W., Chen, Z., Trentesaus, A., Chen, J.F., 2007. Clay minerals in surface sediments of the Pearl River drainage basin and their contribution to the South China Sea. Chin. Sci. Bull. 52 (8), 1101–1111.

Liu, G.H., Zhai, G.Y., Zou, C.N., Cheng, L.J., Guo, X.B., Xia, X.H., Shi, D.S., Yang, Y.R., Zhang, C., Zhou, Z., 2019. A comparative discussion of the evidence for biogenic silica in Wufeng-Longmaxi siliceous shale reservoir in the Sichuan basin, China. Mar. Pet. Geol. 109, 70–87.

Liu, C., Xu, X.Y., Liu, K.Y., Bai, J., Liu, W.B., Chen, S., 2020. Pore-scale oil distribution in shales of the Qingshankou formation in the Changling Sag, Songliao Basin, NE China. Mar. Pet. Geol. 120, 104553. https://doi.org/10.1016/j.marpetgeo.2020.104553.

Lopatin, N.V., Zubairaev, S.L., Kos, I.M., Emets, T.P., Romanov, E.A., Malchikhina, O.V., 2003. Unconventional oil accumulations in the Upper Jurassic Bazhenov Black Shale Formation, West Siberian Basin: a selfsourced reservoir system. J. Pet. Geol. 26 (2), 225–244.

Loucks, R.G., Reed, R.M., Ruppel, S.C., Hammes, U., 2012. Spectrum of pore types and networks in mudrocks and a descriptive classification for matrix-related mudrock pores. AAPG Bull. 96 (6), 1071–1098.

Lu, S.F., Huang, W.B., Chen, F.W., Li, J.J., Wang, M., Xue, H.T., Wang, W.M., Cai, X.Y., 2012. Classification and evaluation criteria of shale oil and gas resources: discussion and application. Pet. Explor. Dev. 39 (02), 249–256. DOI: CNKI:SUN:SKYK.0.2012-02-018.

Lu, S.F., Xue, H.T., Wang, M., Xiao, D.S., Huang, W.B., Li, J.Q., Xie, L.J., Tian, S.S., Wang, S., Li, J.J., Wang, W.M., Chen, F.W., Li, W.H., Xue, Q.Z., Liu, X.F., 2016. Several key issues and research trends in evaluation of shale oil. Acta Pet. Sin. 37 (10), 1309–1322. https://doi.org/10.7623/syxb201610012.

Ma, Y.S., Feng, J.H., 2012. The potential and exploring progress of unconventional hydrocarbon resources in SINOPEC. Eng. Sci. 14 (6), 22–30.

Ma, C.F., Dong, C.M., Luan, G.Q., Lin, C.Y., Liu, X.C., Elsworth, D., 2016. Types, characteristics and effects of natural fluid pressure fractures in shale: a case study of the Paleogene strata in Eastern China. Pet. Explor. Dev. 43 (4), 634–643.

Maende, A., Pepper, A.S., Jarvie, D.M., Weldon, W.D., 2017. Advanced Pyrolysis Data and Interpretation Methods to Identify Unconventional Reservoir Sweet Spots in Fluid Phase Saturation and Fluid Properties (API Gravity) from Drill Cuttings and Cores. Search and Discovery Article #80596.

Mănescu, C.B., Nuño, G., 2015. Quantitative effects of the shale oil revolution. Energy Policy 86, 855–866. https://doi.org/10.2139/ssrn.2622469.

Marchand, A., Libert, P., Combaz, A., 1969. Essai de caracterisation physico-chimique de la diagenese de quelques roches biologiquement homogenes. Rev. Inst. Fr. Pétrol. 24, 3–20.

Matthews, K., Maloney, K., Zahirovic, S., Williams, S., Seton, M., Müller, R., 2016. Global plate boundary evolution and kinematics since the late Paleozoic. Glob. Planet. Chang. 146, 226–250.

McAuliffe, C.D., 1978. Chemical and physical constraints on petroleum migration with emphasis on hydrocarbon solubilities in water. In: Physical and Chemical Constraints on Petroleum Migration. AAPG National Meeting, Oklahoma City 2, p. 39.

Mehana, M., El-monier, I., 2016. Shale characteristics impact on Nuclear Magnetic Resonance (NMR) fluid typing methods and correlations. Petroleum 2, 138–147.

Michael, G.E., Packwood, J., Holba, A., 2013. Determination of in-situ hydrocarbon volumes in liquid rich shale plays. In: SPE/AAPG/SEG Unconventional Resources Technology Conference. Unconventional Resources Technology Conference: 7, Denver, Colorado, USA.

Modiea, C.J., Lapierre, S.G., 2012. Estimation of kerogen porosity in source rocks as a function of thermal transformation:example from the Mowry shale in the Powder river basin of Wyoming. AAPG Bull. 96 (1), 87–108. https://doi.org/10.1306/04111110201.

Mohammadi, M., Sedighi, M., 2013. Modification of Langmuir isotherm for the adsorption of asphaltene or resin onto calcite mineral surface – Comparison of linear and non-linear methods. Protect. Metals Phys. Chem. Surf. 49, 460–470.

Momper, J.A., 1978. Oil migration limitations suggested by geological and geochemical considerations. In: Physical and Chemical Controls on Petroleum Migration: AAPG Continuing Education Course Note Series, No.8. American Association of Petroleum Geologists, Tulsa, pp. B1–B60.

Nie, H.K., Zhang, P.X., Bian, R.K., Wu, X.L., Zhai, C.B., 2016. Enrichment characteristics of continental shale oil in China. Earth Sci. Front. (China Univ. Geosci. (Beijing): Peking Univ.) 23 (02), 55–62. https://doi.org/10.1374/j.esf.2016.02.007.

O'Brien, N.R., Cremer, M.D., Canales, D.G., 2002. The role of argillaceous rock fabric in primary migration of oil. Gulf Coast Assoc. Geol. Soc. Trans. 52, 1103–1112.

Osborne, M.J., Swarbrick, R.E., 1997. Mechanisms for Generating Overpressure in Sedimentary Basins: a Reevaluation. AAPG Bull. 81 (6), 1023–1041.

Pang, X.Q., Chen, Z.M., Chen, F.J., 1993a. Numerical Simulation Study of Geological History, Thermal History, Hydrocarbon Generation and Expulsion History of Petroliferous Basins and Quantitative Evaluation of Source Rocks. Geological Publishing House, Beijing.

Pang, X.Q., Chen, Z.M., Chen, F.J., 1993b. Petroleum-Bearing Basin Geologic History, Thermal History, Generation, Residual and Hydrocarbon-Expulsion History Quantitative Model and Hydrocarbon Source Rocks Quantitative Evaluation. Geological Publishing House, Beijing, pp. 1–160.

Pang, X.Q., Li, M.W., Li, S.M., Jin, Z.J., 2005. Geochemistry of petroleum systems in the Niuzhuang South Slope of Bohai Bay Basin: part 3. Estimating hydrocarbon expulsion from the Shahejie formation. Org. Geochem. 36, 497–510. https://doi.org/10.1016/j.orggeochem.2004.12.001.

Peng, J.W., Pang, X.Q., Shi, H.S., Peng, H.J., Xiao, S., Yu, Q.H., 2016. Hydrocarbon generation and expulsion characteristics of Eocene source rocks in the Huilu area, northern Pearl River mouth basin, South China Sea: implications for tight oil potential. Mar. Pet. Geol. 72, 463–487. https://doi.org/10.1016/j.marpetgeo.2016.02.006.

Pepper, A.S., 1992. Estimating the petroleum expulsion behavior of source rocks: a novel quantitative approach. In: England, W.A., Fleet, A.L. (Eds.), Petroleum migration: Geological Society (London) Special Publication 59, pp. 9–31. https://doi.org/10.1144/GSL.SP.1991.059.01.02.

Pepper, A.S., Corvi, P.J., 1995. Simple kinetic models of petroleum formation. Part I: Oil and gas generation from kerogen. Mar. Pet. Geol. 12 (3), 291–319.

Pepper, A.S., Corvi, P.J., 1995b. Simple kinetic models of petroleum formation. Part III: modelling an open system. Mar. Pet. Geol. 12 (4), 417–452.

Pernyeszi, T., Patzko, A., Berkesi, O., Dekamy, I., 1998. Asphaltene adsorption on clays and crude oil reservoir rocks. Colloids Surf. A Physicochem. Eng. Asp. 137, 373–384.

Peters, K.E., 1986. Guidelines for evaluating petroleum source rock using programmed pyrolysis. AAPG Bull. 70 (3), 318–329.

Peters, K.E., Cassa, M.R., 1994. Applied source rock geochemistry. In: Magoon, L.B., Dow, W.G. (Eds.), The Petroleum System: From Source to Trap. American Association of Petroleum Geologists, Tulsa, pp. 93–120.

Philippi, G.T., 1965. On the depth, time and mechanism of petroleum generation. Geochim. Cosmochim. Acta 29, 1021–1049.

Plimpton, S., 1995. Fast parallel algorithms for short-range molecular dynamics. J. Comput. Phys. 117 (1), 1–19.

Qian, M.H., Jiang, Q.G., Li, M.W., Li, Z.M., Liu, P., Ma, Y.Y., Cao, T.T., 2017. Quantitative characterization of extractable organic matter in lacustrine shale with different occurrences. Pet. Geol. Exp. 39 (02), 278–286. https://doi.org/10.11781/sysydz201702278.

Ribeiro, R.C., Correia, J.C.G., Seidl, P.R., 2009. The influence of different minerals on the mechanical resistance of asphalt mixtures. J. Pet. Sci. Eng. 65, 171–174.

Roberts, S.J., Nunn, D.F., 1995. Episodic fluid expulsion from geopressured sediments. Mar. Pet. Geol. 12, 195–204.

Romero-Sarmiento, M.-F., Pillot, D., Letort, G., Lamoureux-Var, V., Beaumont, V., Huc, A.-Y., Garcia, B., 2016. New rock-eval method for characterization of unconventional shale resource systems. Oil Gas Sci. Technol. Rev. IFP Energies nouvelles 71 (37), 1–9.

Rowe, H.D., Loucks, R.G., Ruppel, S.C., Rimmer, S.M., 2008. Mississippian Barnett Formation, FortWorth Basin, Texas: bulk geochemical inferences and Mo-TOC constraints on the severity of hydrographic restriction. Chem. Geol. 257, 16–25.

Sandvik, E.I., Young, W.A., Curry, D.J., 1992. Expulsion from hydrocarbon sources: the role of organic absorption. Org. Geochem. 19 (1–3), 77–87. https://doi.org/10.1016/0146-6380(92)90028-V.

Sanei, H., Wood, J.M., Ardakani, O.H., Clarkson, C.R., Jiang, C.Q., 2015. Characterization of organic matter fractions in an unconventional tight gas siltstone reservoir. Int. J. Coal Geol. 150-151, 296–305.

Shao, X.H., Pang, X.Q., Li, H., Hu, T., Xu, T.W., Xu, Y., Li, N.Y., 2018. Pore network characteristics of lacustrine shales in the Dongpu Depression, Bohai Bay Basin, China, with implications for oil retention. Mar. Pet. Geol. 96, 457–473. https://doi.org/10.1016/j.marpetgeo.2018.06.015.

Sing, K.S., Everett, D.H., Haul, R.A.W., Moscou, L., Pierotti, R.A., Rouquerol, J., Siemieniewsha, T., 1985. Reporting physisorption data for gas/solid systems with special reference to the determination of surface area and porosity. Pure Appl. Chem. 57 (4), 603–619.

Song, G.Q., Zhang, L.Y., Lu, S.F., Xu, X.Y., Zhu, R.F., Wang, M., Li, Z., 2013. Resource evaluation method for shale oil and its application. Earth Sci. Front. (China Univ. Geosci. (Beijing): Peking Univ.) 20 (04), 221–228. DOI: CNKI: SUN: DXQY. 0.2013–04-021.

Stainforth, J.G., 2009. Practical kinetic modelling of petroleum generation and expulsion. Mar. Pet. Geol. 26, 552–572. https://doi.org/10.1016/j.marpetgeo.2009.01.006.

Su, S.Y., Jiang, Z.X., Gao, Z.Y., Ning, C.X., Wang, Z., Li, Z., Zhu, R.F., 2017a. A new method for continental shale oil enrichment evaluation. Interpretation 5 (2), 1–9. https://doi.org/10.1190/INT-2016-0158.1.

Su, S.Y., Jiang, Z.X., Ning, C.X., Wang, Z., Li, Z., Zhu, R.F., 2017b. Study of the main controlling factors of shale oil enrichment in the Zhanhua Sag. Petrol. Sci. Bull. 2 (02), 187–198. https://doi.org/10.3969/j.issn.2096-1693.2017.02.018.

Surdam, R.C., Crossey, L.J., Hagen, E.S., 1989. Organic-inorganic and sandstone diagenesis. AAPG Bull. 73, 1–23.

Tang, L., Song, Y., Pang, X.Q., Jiang, Z.X., Guo, Y.C., Zhang, H.G., Pan, Z.H., Jiang, H., 2020. Effects of paleo sedimentary environment in saline lacustrine basin on organic matter accumulation and preservation: a case study from the Dongpu Depression, Bohai Bay Basin, China. J. Pet. Sci. Eng. 185, 106669. https://doi.org/10.1016/j.petrol.2019.106669.

Tian, S.S., Xue, H.T., Lu, S.F., Zeng, F., Xue, Q.Z., Chen, G.H., Wu, C.Z., Zhang, S.S., 2017. Molecular simulation of oil mixture adsorption character in shale system. J. Nanosci. Nanotechnol. 17 (9), 6198–6209.

Van, H.K.H., 2000. Progress of coal science in the 20th century. Fuel 79 (1), 1–26. https://doi.org/10.1016/S0016-2361(99)00190-8.

Wang, Z.Y., Cheng, K.M., 2000. The organic geochemical characteristics comparison and contributors of different existing state organic matter in carbonate rocks. Acta Sedimentol. Sin. 18 (4), 600–605.

Wang, M., Sherwood, N., Li, Z.S., Lu, S.F., Wang, W.G., Huang, A.H., Peng, J., Lu, K., 2015a. Shale oil occurring between salt intervals in the Dongpu Depression, Bohai Bay Basin, China. Int. J. Coal Geol. 152, 100–112. https://doi.org/10.1016/j.coal.2015.07.004.

Wang, S., Feng, Q.H., Zha, M., Lu, S.F., Qin, Y., Xia, T., Zhang, C., 2015b. Molecular dynamics simulation of liquid alkane occurrence state in pores and slits of shale organic matter. Pet. Explor. Dev. 42 (6), 84–851. https://doi.org/10.1016/S1876-3804(15)30081-1.

Wang, M., Wilkins, R.W.T., Song, G.Q., Zhang, L.Y., Xu, X.Y., Li, Z., Chen, G.H., 2015c. Geochemical and geological characteristics of the Es3L lacustrine shale in the Bonan sag, Bohai Bay Basin, China. Int. J. Coal Geol. 138, 16–29. https://doi.org/10.1016/j.coal.2014.12.007.

Wang, W.G., Zheng, M., Wang, M., Lu, S.F., Peng, J., Lu, K., Wu, X.Z., Huang, A.H., 2015d. Discussion on evaluation method of shale oil movable resource and its application in Shahejie Formation of Paleogene in northern Dongpu. Sag. Nat. Gas Geosci. 26 (4), 771–781.

Wang, S., Javadpour, F., Feng, Q.H., 2016a. Fast mass transport of oil and supercritical carbon dioxide through organic nanopores in shale. Fuel 181, 741–758. https://doi.org/10.1016/j.fuel.2016.05.057.

Wang, S., Javadpour, F., Feng, Q.H., 2016b. Molecular dynamics simulations of oil transport through inorganic nanopores in shale. Fuel 171, 74–86. https://doi.org/10.1016/j.fuel.2015.12.071.

Wang, Q., Song, X.X., Li, R.R., 2018. A novel hybridization of nonlinear grey model and linear ARIMA residual correction for forecasting U.S. shale oil production. Energy 165, 1320–1331. https://doi.org/10.1016/j.energy.2018.10.032.

Wang, M., Li, J.B., Guo, Z.Q., Li, C.M., Lu, S.F., 2018c. An organic-rich mud shale hydrogen content, porosity and pore size evaluation method. China Patent NO. 2018102604080. Shandong: China.

Wang, M., Guo, Z.Q., Jiao, C.X., Lu, S.F., Li, J.B., Xue, H.T., Li, J.J., Li, J.Q., Chen, G.H., 2019a. Exploration progress and geochemical features of lacustrine shale oils in China. J. Pet. Sci. Eng. 178, 975–986. https://doi.org/10.1016/j.petrol.2019.04.029.

Wang, S., Feng, Q.H., Javadpour, F., Hu, Q.H., Wu, K.L., 2019b. Competitive adsorption of methane and ethane in montmorillonite nanopores of shale at supercritical conditions: a grand canonical Monte Carlo simulation study. Chem. Eng. J. 355, 76–90. https://doi.org/10.1016/j.cej.2018.08.067.

Wang, W.Y., Pang, X.Q., Chen, Z.X., Chen, D.X., Ma, X.H., Zhu, W.P., Zheng, T.Y., Wu, K. L., Zhang, K., Ma, K.Y., 2020. Improved methods for determining effective sandstone reservoirs and evaluating hydrocarbon enrichment in petroliferous basins. Appl. Energy 261, 114457. https://doi.org/10.1016/j.apenergy.2019.114457.

Wang, K., Pang, X.Q., Zhang, H.A., Hu, T., Xu, T.W., Zheng, T.Y., Zhang, X.W., 2020a. Organic geochemical and petrophysical characteristics of saline lacustrine shale in the Dongpu Depression, Bohai Bay Basin, China: Implications for Es3 hydrocarbon exploration. J. Pet. Sci. Eng. 184, 106546. https://doi.org/10.1016/j.petrol.2019.106546.

Williams, J.L.A., Taylor, D.G., Maddinelli, G., Enwere, P., Archer, J.S., 1991. Visualisation of fluid displacement in rock cores by NMR imaging. Magn. Reson. Imaging 9 (5), 767–773.

Wu, L.Y., Zhang, Z.L., Ma, W.L., 2000. Quantitative analysis method for reservoir rock oil and gas component. Mud Logging Eng. 11 (3), 50–58.

Wu, G.X., Wang, Z.P., Sun, J.B., Wang, S.J., 2003. Problem Discussion on Evaluation of Continental Source Rocks (in Chinese with English Abstract): Fault-Block Oil and Gas Field 10, pp. 28–31.

Wu, C.J., Zhang, M.F., Ma, W.Y., Liu, Y., Xiong, D.M., Sun, L.N., Tuo, J.C., 2014. Organic matter characteristic and sedimentary environment of the lower Cambrian Niutitang Shale in Southeastern Chongqing. Nat. Gas Geosci. 25 (08), 1267–1274. https://doi.org/10.11764/j.issn.1672-1926.2014.08.1267.

Xue, H.T., Tian, S.S., Lu, S.F., Zhang, W.H., Du, T.T., Mu, G.D., 2015. Selection and verification of key parameters in the quantitative evaluation of shale oil:a case study at the Qingshankou Formation , Northern Songliao Basin. Bull. Mineral. Petrol. Geochem. 34 (1), 70–78. https://doi.org/10.3969/j.issn.1007-2802.2015.01.008.

Xue, H.T., Tian, S.S., Wang, W.M., Zhang, W.H., Du, T.T., Mu, G.D., 2016. Correction of oil content—One key parameter in shale oil resource assessment. Oil Gas Geol. 37 (1), 15–22. https://doi.org/10.11743/ogg20160103.

Yuan, M.H., Idris, A.K., 1995. Role of asphaltene in changing wettability of reservoir rock. In: Proceedings of the Eleventh Symposium of Malaysia Chemical Engineers, C12-1.

Yuan, G.H., Cao, Y.C., Schulz, H.M., Hao, F., Gluyas, J., Liu, K.Y., Yang, T., Wang, Y.Z., Xi, K.L., Li, F.L., 2019. A review of feldspar alteration and its geological significance in sedimentary basins: from shallow aquifers to deep hydrocarbon reservoirs. Earth Sci. Rev. 191, 114–140. https://doi.org/10.1016/j.earscirev.2019.02.004.

Yurewicz, D.A., Bohacs, K.M., Bohacs, K.M., Klimentidis, R.E., Meurer, M.E., Yeakel, J.D., Ryan, T.C., Kendall, J., 2008. Controls on gas and water distribution, Mesaverde basin-centered gas play, Piceance Basin, Colorado. In: Cumella, S.P., Shanley, K.W., Camp, W.K. (Eds.), Understanding, Exploring, and Developing Tight-Gas Sands - 2005 Vail Hedberg Conference, AAPG Hedberg Series, vol. 3, pp. 105–136.

Zhang, Z.L., Wu, L.Y., Tuo, Q., Shu, L.Z., 2007. Abnormal value recovery of maturity parameter T_{max} for Rock-Eval. Pet. Explor. Dev. 34 (5), 580–584.

Zhang, J.C., Lin, L.M., Li, Y.X., Tang, X., Zhu, L.L., Xing, Y.W., Jiang, S.L., Jing, T.Y., Yang, S.Y., 2012. Classification and evaluation of shale oil. Earth Sci. Front. 19 (5), 322–331.

Zhang, L.Y., Bao, Y.S., Li, J.Y., Li, Z., Zhu, R.F., Zhang, J.G., 2014. Movability of lacustrine shale oil: a case study of Dongying Sag, Jiyang Depression, Bohai Bay Basin. Pet. Explor. Dev. 41 (6), 703–711. https://doi.org/10.1016/S1876-3804(14)60084-7.

Zhang, J., Lu, K., Jiang, F.H., Shi, X.H., Tian, J.T., Cao, H.M., Guo, H., 2015. Enrichment condition of shale oil and gas in Dongpu Depression. Fault-Block Oil Gas Field 22 (02), 184–188. https://doi.org/10.6056/dkyqt201502010.

Zhao, W.Z., Hu, S.Y., Hou, L.H., Yang, T., Li, X., Guo, B.C., Yang, Z., 2020a. Types and resource potential of continental shale oil in China and its boundary with tight oil. Pet. Explor. Dev. 47 (1), 1–11. https://doi.org/10.1016/S1876-3804(20)60001-5.

Zhao, X.Z., Pu, X.G., Zhou, L.H., Jin, F.M., Shi, Z.N., Han, W.Z., Jiang, W.Y., Zhang, W., 2020b. Typical geological characteristics and exploration practices of lacustrine shale oil: a case study of the Kong-2 member strata of the Cangdong Sag in the Bohai Bay Basin. Mar. Pet. Geol. 113, 103999. https://doi.org/10.1016/j.marpetgeo.2019.08.027.

Zhou, S.W., Yan, G., Xue, H.Q., Guo, W., Li, X.B., 2016. 2D and 3D nanopore characterization of gas shale in Longmaxi formation based on FIB-SEM. Mar. Pet. Geol. 73, 174–180.

Zhu, X.J., Cai, J.G., 2012. Progress and significance of research on relation between specific surface area and organic matter in argillaceous source rocks. Oil Gas Geol. 33 (3), 375–384.

Zhu, G.Y., Jing, Q., 2003. Geochemical characteristics of two sets of excellent source rocks in. Dongying Depress. Acta Sedimentol. Sin. 21 (3), 506–512.

Zhu, R.F., Zhang, L.Y., Li, J.Y., Liu, Q., Li, Z., Wang, R., Zhang, L., 2015. Quantitative Evaluation of Residual Liquid Hydrocarbons in Shale. Acta Pet. Sin. 36 (1), 13–18. https://doi.org/10.7623/syxb201501002.

Zhu, X.M., Zhu, W.B., Cao, J., Song, Y., Zhang, D.M., Hu, S.Z., Li, S.F., 2019a. Research progress on shale oil mobility characterization. Xinjiang Petr. Geol. 40 (06), 745–753. https://doi.org/10.7657/XJPG20190617.

Zhu, X.J., Cai, J.G., Liu, Q., Li, Z., Zhang, X.J., 2019b. Thresholds of petroleum content and pore diameter for petroleum mobility in shale. AAPG Bull. 103, 605–617.

Zou, C.N., Yang, Z., Cui, J.W., Zhu, R.K., Hou, L.H., Tao, S.Z., Yuan, X.J., Wu, S.T., Lin, S. H., Wang, L., Bai, B., Yao, J.L., 2013. Formation mechanism, geological characteristics and development strategy of nonmarine shale oil in China. Pet. Explor. Dev. 40 (1), 15–27. https://doi.org/10.1016/S1876-3804(13)60002-6.

Zou, C.N., Zhu, R.K., Chen, Z.Q., Ogg, J.G., Wu, S.T., Dong, D.Z., Qiu, Z., Wang, Y.M., Wang, L., Lin, S.H., Cui, J.W., Su, L., Yang, Z., 2019. Organic-matter-rich shales of China. Earth Sci. Rev. 189, 51–78. https://doi.org/10.1016/j.earscirev.2018.12.002.